Biogeochemical Niches of Fe-Cycling Communities Influencing Heavy Metal Transport along the Rio Tinto, Spain

Sergey M. Abramov,[a,b] Daniel Straub,[a,c] Julian Tejada,[d*] Lars Grimm,[b] Franziska Schädler,[a,b] Aleksandr Bulaev,[e] Harald Thorwarth,[d] Ricardo Amils,[f] Andreas Kappler,[b,g] Sara Kleindienst[a]

[a]Microbial Ecology, Center for Applied Geosciences, University of Tuebingen, Tuebingen, Baden-Württemberg, Germany
[b]Geomicrobiology, Center for Applied Geosciences, University of Tuebingen, Tuebingen, Baden-Württemberg, Germany
[c]Quantitative Biology Center, University of Tuebingen, Tuebingen, Baden-Württemberg, Germany
[d]University of Applied Forest Sciences Rottenburg, Rottenburg am Neckar, Baden-Württemberg, Germany
[e]Winogradsky Institute of Microbiology, Research Center of Biotechnology of the Russian Academy of Sciences, Moscow, Russia
[f]Centre for Molecular Biology Severo Ochoa, Autonomous University of Madrid, Madrid, Spain
[g]Cluster of Excellence EXC 2124, Controlling Microbes to Fight Infection, Tuebingen, Baden-Württemberg, Germany

ABSTRACT   In the mining-impacted Rio Tinto, Spain, Fe-cycling microorganisms influence the transport of heavy metals (HMs) into the Atlantic Ocean. However, it remains largely unknown how spatial and temporal hydrogeochemical gradients along the Rio Tinto shape the composition of Fe-cycling microbial communities and how this in turn affects HM mobility. Using a combination of DNA- and RNA-based 16S rRNA (gene) amplicon sequencing and hydrogeochemical analyses, we explored the impact of pH, Fe(III), Fe(II), and Cl⁻ on Fe-cycling microorganisms. We showed that the water column at the acidic (pH 2.2) middle course of the river was colonized by Fe(II) oxidizers affiliated with *Acidithiobacillus* and *Leptospirillum*. At the upper estuary, daily fluctuations of pH (2.7 to 3.7) and Cl⁻ (6.9 to 16.6 g/L) contributed to the establishment of a unique microbial community, including Fe(II) oxidizers belonging to *Acidihalobacter*, *Marinobacter*, and *Mariprofundus*, identified at this site. Furthermore, DNA- and RNA-based profiles of the benthic community suggested that acidophilic and neutrophilic Fe(II) oxidizers (e.g., *Acidihalobacter*, *Marinobacter*, and *Mariprofundus*), Fe(III) reducers (e.g., *Thermoanaerobaculum*), and sulfate-reducing bacteria drive the Fe cycle in the estuarine sediments. RNA-based relative abundances of *Leptospirillum* at the middle course as well as abundances of *Acidihalobacter* and *Mariprofundus* at the upper estuary were higher than DNA-based results, suggesting a potentially higher level of activity of these taxa. Based on our findings, we propose a model of how tidal water affects the composition and activity of the Fe-cycling taxa, playing an important role in the transport of HMs (e.g., As, Cd, Cr, and Pb) along the Rio Tinto.

IMPORTANCE   The estuary of the Rio Tinto is a unique environment in which extremely acidic, heavy metal-rich, and especially iron-rich river water is mixed with seawater. Due to the mixing events, the estuarine water is characterized by a low pH, almost seawater salinity, and high concentrations of bioavailable iron. The unusual hydrogeochemistry maintains unique microbial communities in the estuarine water and in the sediment. These communities include halotolerant iron-oxidizing microorganisms which typically inhabit acidic saline environments and marine iron-oxidizing microorganisms which, in contrast, are not typically found in acidic environments. Furthermore, highly saline estuarine water favored the prosperity of acidophilic heterotrophs, typically inhabiting brackish and saline environments. The Rio Tinto estuarine sediment harbors a diverse microbial community with both acidophilic and neutrophilic members that can mediate the iron cycle and, in turn, can directly impact the mobility and transport of heavy metals in the Rio Tinto estuary.

KEYWORDS   Rio Tinto, acidophiles, estuary, extremophiles, heavy metals, microbial communities, microbial ecology

The Rio Tinto has been the focus of systematic geomicrobiological explorations since 1980 (1). Many detailed surveys of the unique microbial communities inhabiting the river and their impact on the water hydrogeochemistry have been conducted over the past 3 decades (2–5). These studies demonstrated the role of prokaryotes and fungi in the precipitation of minerals by providing nucleation sites (e.g., charged surfaces or extracellular polymeric substances). Nucleation sites favor the precipitation of Fe minerals by overcoming kinetic barriers in acidic water, which is characterized by slow precipitation kinetics (6–10). The precipitation of dissolved Fe in close proximity of the cells leads to formation of cell-mineral aggregates consisting of Fe(III) (oxyhydr)oxides (e.g., ferrihydrite), Fe(III) hydroxysulfates (e.g., schwertmannite and jarosite), and Fe(II) carbonates (e.g., siderite) and coprecipitation or sorption of other metals (e.g., Cr, Pb, etc.) and metalloids (e.g., As, etc.) (6, 10–14) which can be grouped into the category of heavy metals (HMs) according to the toxicity criterion (15, 16). Produced cell-mineral aggregates can remain suspended in the water column and enter the ocean with the dissolved metals (e.g., Zn, Cd, and Mn) (17–19). Although most elements are transported to the ocean exclusively in the dissolved phase, Fe, Pb, Cr, and As are associated with a large quantity of suspended particulate matter (SPM) (20, 21). The HMs transported to the coastal water in the SPM-associated form can be toxic to marine organisms (19, 22–26). Therefore, studying the mechanisms of Fe mineral formation and HM transport is important for the ecology of the coastal-estuarine zone of southwestern Spain (19, 27–31). The precipitation of Fe(III) minerals in the acidic Rio Tinto occurs after microbially mediated Fe(II) oxidation oversaturates the water with dissolved Fe(III) (21). In the river water, typically >60% of 16S rRNA (gene) sequences belonged to Fe(II)-oxidizing *Acidithiobacillus* and *Leptospirillum*, making them the main drivers of Fe(III) oversaturation in the water (32, 33). Together with fungi and algae, they provide sites for nucleation and ordering of Fe(III) minerals (34). The precipitation of Fe(II) minerals (e.g., siderite) is related to the microbial reduction of Fe(III), coupled to the oxidation of organic compounds by Fe(III)-reducing *Acidiphilium* (10). Dissimilatory Fe(III)-reducers affiliating with *Acidiphilium* and *Acidibacter* are typically represented by >10% of 16S rRNA (gene) sequences (32, 33). Furthermore, the dissimilatory microbial Fe(III) reduction plays an important role in recharging of the water with Fe(II) and removal of organic compounds (e.g., acetate, lactate, pyruvate, formate, and propionate) which inhibit chemolithoautotrophic growth of Fe(II) oxidizers (35–37).

Thus, *Leptospirillum*, *Acidithiobacillus*, *Acidiphilium*, and *Acidibacter* are highly abundant in the Rio Tinto and play an important role in Fe mineralization and HM mobility. They can also influence the fate of SPM-associated HMs. For example, microbial cells attached to particles can be significantly more productive than their planktonic counterparts (38). Particle-associated microorganisms can efficiently degrade particulate organic molecules associated with HMs (39) and therefore play an important role in the remineralization of SPM-associated HMs. However, it is largely unknown how both planktonic and particle-associated fractions of microorganisms react to spatial and temporal hydrogeochemical gradients forming at the upper estuary due to tidal activity of the ocean (40–43). The characteristic features of this part of the river are longitudinal (2.5 to 7.0) and temporal gradients of the pH and chlorinity (1.7 to 19.5 g/L) of water as well as high concentrations of dissolved HMs. At the upper estuary, the neutralization process results in the precipitation of sulfate salts, which scavenge dissolved HMs transported by the Rio Tinto. Furthermore, elevated pH values facilitate the abiotic oxidation of dissolved Fe(II) and the precipitation of Fe(III) minerals (44). Tidal activity can lead to unfavorable conditions [e.g., elevated pH and Cl^- concentration, as well as diminishing Fe(II) and Fe(III) concentrations] that can inhibit the growth of acidophiles (45). Therefore, there are several open questions regarding the abundance and activity of Fe-cycling microorganisms at the water column of the upper estuary. Furthermore, much less research has focused on the composition of the benthic microbial community at the estuary of the river and the role of benthic microorganisms in the fate of HMs (46).

In order to reveal how the spatial (along the river) and temporal (at the upper estuary) hydrogeochemical fluctuations affect the diversity and abundance of microorganisms responsible for Fe redox transformations influencing the fate of HMs, we identified and compared

diurnal hydrogeochemical parameters that are typical of the summer season at the middle course and at the upper estuary of the Rio Tinto. In addition, we examined and compared the composition of planktonic, particle-associated, and benthic microbial communities at both field sites and identified microbial key players involved in Fe cycling in different biogeochemical niches. The application of only 16S rRNA gene sequencing for microbial community analyses can lead to false-positive results because of the inability to differentiate live cells (dormant cells as well as growing or nongrowing metabolically active cells) and present cells (dead cells and extracellular DNA) (47). To discriminate between live and present microorganisms, along with DNA-based 16S rRNA gene amplicon sequencing, we applied RNA-based amplicon sequencing, which is commonly used for identification of *in situ* alive microbial taxa (47–51). Both dormant and metabolically active cells produce rRNA; however, in dormant cells, ribosomes and rRNA decrease to minimal levels (49). Another advantage of the RNA-based approach is the high degradation rate of RNA in the environment (compared to DNA), which reduces the chance to obtain false-positive results of microbial community analysis (47). Finally, we provide insights into the potential interrelationships of Fe-cycling communities with HMs, commonly associated with particulate transport (e.g., As, Cr, Cd, and Pb).

RESULTS

Water hydrogeochemistry at the middle course and upper estuary of the Rio Tinto. Triplicate samples of the river water were collected every 2 h over 2 days at the middle course and 1 day at the upper estuary (Fig. 1a and b). Hydrogeochemical parameters of the water at both sampling sites are provided in Table 1. At the middle course, we quantified 19 mg/L (day 1) and 33 mg/L (day 2) of dissolved Fe(II), while the concentration of dissolved Fe(III) reached 2,234 mg/L (day 1) and 2,369 mg/L (day 2). Concentrations of Cl^- were comparatively low over 2 days (ca. 34 mg/L). The pH of the water remained consistently low (2.2) over the 2 days, while the E_h value varied from 790 mV (day 1) to 785 mV (day 2). At the upper estuary, we observed a fluctuation of the pH from 2.7 (low tide) to 3.7 (high tide). The E_h value also fluctuated from 645 mV (low tide) to 526 mV (high tide). Concentrations of Na^+ and Cl^- were 3,558 mg/L and 6,902 mg/L during low tide and 8,619 mg/L and 16,571 mg/L during high tide, respectively. Concentrations of dissolved Fe(III) were much lower at the upper estuary, 6.6 mg/L (low tide) and 2.9 mg/L (high tide). We also observed a decrease of the Fe(II) concentration to 9.4 mg/L (low tide) and 2.8 mg/L (high tide). Nitrate concentrations were very similar at both field sites. At the middle course, we quantified 31 and 29 mg/L of NO_3^-, while at the upper estuary, NO_3^- decreased to 22.4 and 15.2 mg/L during high tide and low tide, respectively. Concentrations of O_2 were relatively stable (6.6 mg/L to 6.8 mg/L) at the middle course, while at the upper estuary it reached 11.6 mg/L (low tide) and 11.4 mg/L (high tide).

Concentrations of dissolved Cr, As, Pb, and Cd at the middle course were 0.003 to 0.002, 1.52 to 1.35, 0.05 to 0.04, and 1.05 to 0.94 mg/L, respectively (Fig. 2a). At the upper estuary, As and Cr were not detectable in the dissolved phase. Pb (0.08 and 0.04 mg/L during low tide and high tide, respectively) was found at almost equal concentrations determined at the middle course (0.05 and 0.04 mg/L during day 1 and day 2, respectively). Furthermore, Cd (0.04 and 0.02 mg/L during low tide and high tide, respectively) was significantly removed from the estuarine water compared with the dissolved content at the middle course (1.05 and 0.94 mg/L during day 1 and day 2, respectively) (Fig. 2b).

At the middle course, we quantified 0.86, 3.04, 7.78, and 0.46 μg/L of SPM-associated Cr, As, Pb, and Cd, respectively, during day 1 and 0.41, 3.85, 9.54, and 0.71 μg/L, respectively, during day 2 using water filtration through 0.45-μm-pore-size filters (Fig. 2c). At the upper estuary, we quantified 1.01, 5.78, 1.81, and 0.05 μg/L of Cr, As, Pb, and Cd, respectively, during low tide and 2.17, 9.57, 2.16, and 0.005 μg/L of Cr, As, Pb, and Cd, respectively, during high tide (Fig. 2d). Furthermore, we observed an increase in average SPM content at the upper estuary during high and low tide compared with the middle course (Fig. 2e).

Minerology of estuarine sediment. Iron-containing minerals in the estuarine sediments ES1 and ES2 were identified in our previous study (21). Here, using micro-X-ray diffraction (μ-XRD) analysis, we determined the mineralogy of the red plaques (ES-RP) sampled from the sediment ES4 (Fig. 1b). The plaques were dominated by two crystalline mineral phases, i.e., quartz and goethite (see Fig. S1 in the supplemental material).
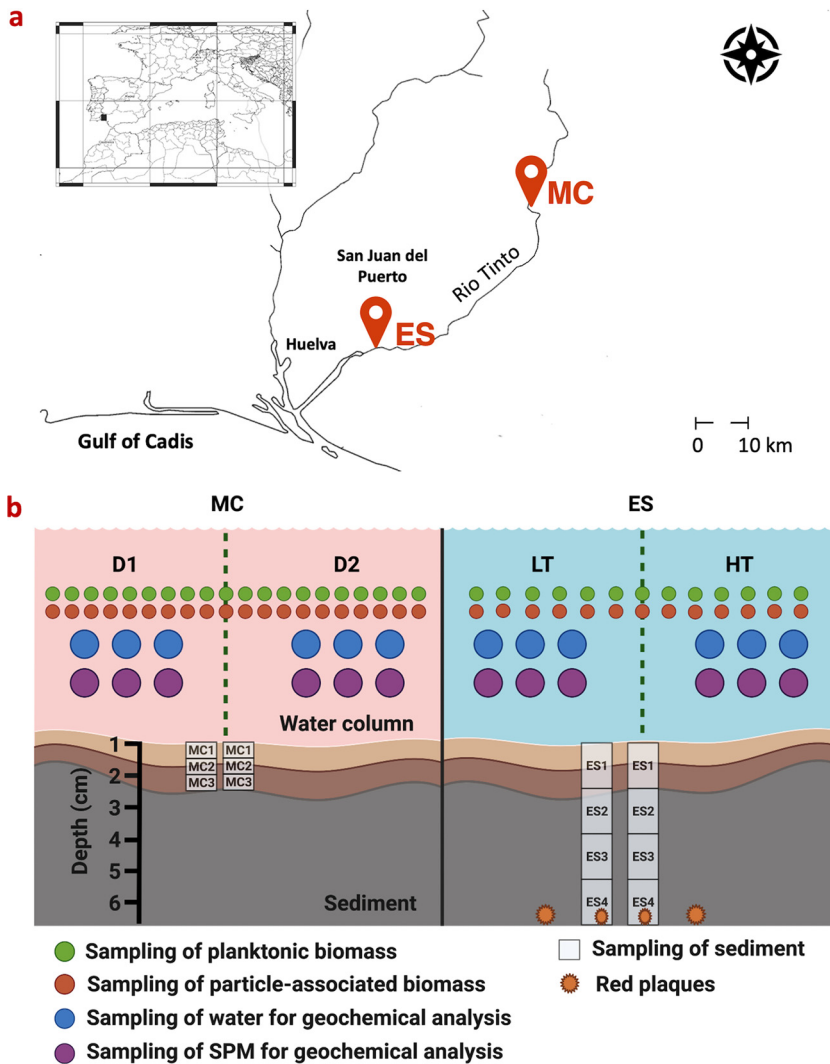
FIG 1 Field sites located at the middle course (MC) and upper estuary (ES) of the Rio Tinto selected for sampling water and sediment. (a) Geographical cartography of the Rio Tinto basin with two selected sampling sites (MC and ES; map created with QGIS version 2.14.0 [http://www.qgis.org/en/site/]). (b) Schematic illustration of sampling at the MC during day 1 (D1) and day 2 (D2) and at the ES during low tide (LT) and high tide (HT) (created with BioRender.com).

Microbial communities of the middle course and upper estuary of the Rio Tinto. We identified DNA- and RNA-based 16S rRNA (gene) relative abundances of microbial taxa in the water column and sediment at both sampling sites (Fig. 3 and 4 and Data Sets S2 and S3). The highest community richness (defined by the number of amplicon sequence variants [ASVs]) and diversity (measured by the Shannon diversity index) were determined in sediment samples of the upper estuary (Fig. S2 to S5). Relative abundances of specific taxa represent average values of triplicate samples of planktonic and particle-associated fractions and duplicate samples of benthic fractions, except of benthic samples MC3, ES1, and ES-RP, for which only one successful extraction was possible (Fig. 1b). In order to discriminate between live (potentially active) and present microorganisms, the DNA- and RNA-based relative abundances of taxa including microorganisms known for their capabilities for Fe redox transformations were analyzed individually (Fig. 5 and Data Set S4). Results of 16S rRNA (gene) sequencing demonstrated that at the middle course of the Rio Tinto, the DNA-based relative abundances of acidophilic Fe(II)-oxidizing *Acidithiobacillaceae* (40.6 to 62.0%), Fe(III)-reducing *Acetobacteraceae* (10.4 to 10.7%), and the potential human pathogens unclassified *Legionellaceae* (14.7 to 34.2%) were dominant in the planktonic fraction over 2 days of sampling. RNA-based relative abundances revealed Fe(II)-oxidizing *Acidithiobacillaceae* (40.1 to

TABLE 1 Physicochemical characteristics of the water[a]

Parameter	MC-D1		MC-D2		ES-LT		ES-HT	
	Mean	SD	Mean	SD	Mean	SD	Mean	SD
pH	2.2	0.2	2.2	0.1	2.704	0.005	3.7	0.2
O_2 (mg/L)	6.6	0.3	6.8	0.4	11.6	4.5	11.4	0.2
Salinity (g/L)	5.7	0.1	5.7	0.2	11.7	0.4	27.7	0.5
E_h (mV)	790.4	2.2	785.2	9.6	645.0	17.0	526.0	15.5
Fe(II) (mg/L)	19.1	1.5	32.9	18.4	9.4	1.1	2.8	1.4
Fe(III) (mg/L)	2,233.5	133.7	2,369.0	118.0	6.6	1.3	2.9	2.0
Cl^- (mg/L)	33.5	NA	34.0	NA	6,902.4	49.6	16,571.2	94.5
SO_4^{2-} (mg/L)	5,048.0	NA	5,012.0	NA	2,362.2	43.6	3,130.9	45.7
NO_3^- (mg/L)	31.2	NA	29.2	NA	22.4	6.8	15.2	2.0
Na (mg/L)	46.6	4.2	42.5	1.5	3,557.7	77.8	8,618.7	278.7

[a]Characteristics were assessed at the middle course during days 1 and 2 (MC-D1 and MC-D2) and at the upper estuary during low tide and high tide (ES-LT and ES-HT). Mean values were calculated based on triplicate water samples collected every 2 h during days 1 and 2 at the middle course and triplicate water samples collected during two high and two low tides at the upper estuary (see Data Set S1). NA, not applicable.

44.7%) and *Nitrospiraceae* (23.7 to 29.5%) as well as Fe(III)-reducing *Acetobacteraceae* (14.1 to 16.0%) as the most dominant, potentially active taxa in the planktonic fraction. The particle-associated microbial community was dominated by *Acidithiobacillaceae* (17.4 to 34.4%), *Nitrospiraceae* (6.9 to 11.0%) and *Legionellaceae* (37.6 to 47.3%) at the DNA-based level and by *Acidithiobacillaceae* (22.6 to 30.7%), *Nitrospiraceae* (27.4 to 29.8%), *Legionellaceae* (12.1 to 21.3%), and *Acetobacteraceae* (11.6 to 13.7%) at the RNA-based level (Fig. 3 and Data Set S2).

In the middle course, the benthic microbial community was dominated by Fe-cycling microorganisms. At MC2 sediment, *Nitrospiraceae* (17.5%), *Rhodanobacteraceae* (25.5%), and *Acidibacter* (order *Gammaproteobacteria*; 10.7%) dominated at the DNA-based level, while in the RNA-based microbial community, *Nitrospiraceae* (13.9%), *Acetobacteraceae* (18.3%), *Rhodanobacteraceae* (11.3%), *Acidibacter* (13.7%), and *Acidiferrobacteraceae* (10.4%) were the most dominant taxa. At MC3 sediment, *Nitrospiraceae*, *Acetobacteraceae*, and *Acidibacter* domi-
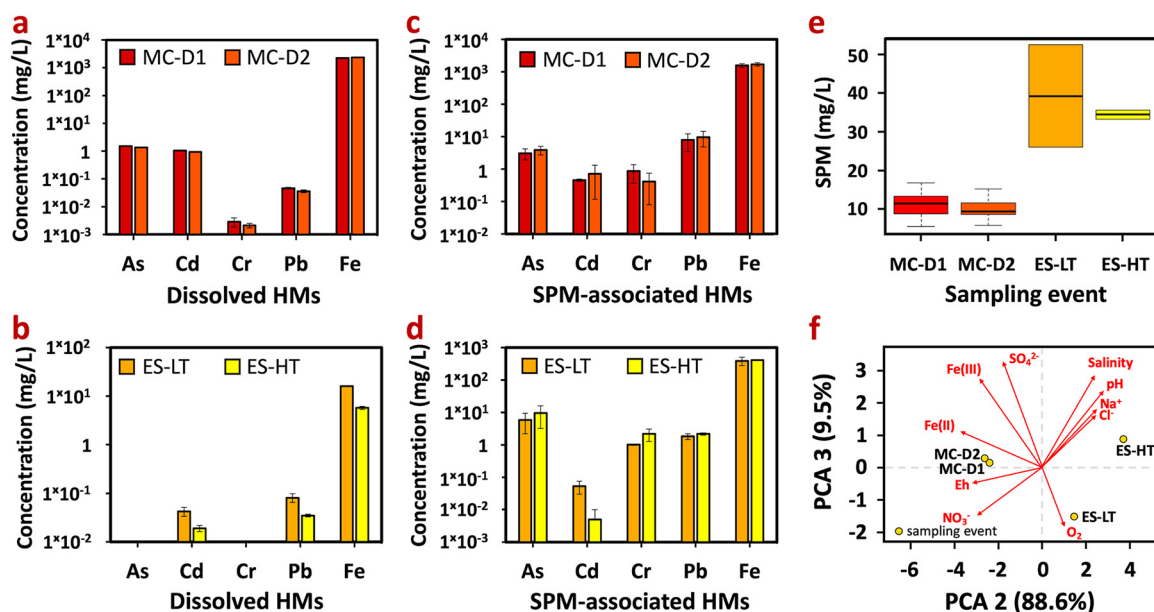
FIG 2 Physicochemical characteristics of the water column at the middle course (MC) sampled at day 1 (MC-D1) and day 2 (MC-D2) as well as at the upper estuary (ES) sampled during low tide (ES-LT) and high tide (ES-HT). (a to d) Content of As, Cr, Cd, Pb, and total Fe in suspended particulate matter (SPM)-associated (>0.45-µm-grain-size) and dissolved fractions of the water column at both sampling sites during four sampling events: MC-D1 (13 samples), MC-D2 (13 samples), ES-LT (2 samples), and ES-HT (2 samples; adapted from reference 21; also, see Data Set S1). (e) Content of SPM (>0.45 µm grain size) in the water column of MC-D1 (13 samples), MC-D2 (13 samples), ES-LT (2 samples), and ES-HT (2 samples). (f) Principal-component analysis (PCA) plot of hydrogeochemical data (Table 1) determined in the river water during MC-D1, MC-D2, ES-LT, and ES-HT. The second and third principal components (PCA 2 and PCA 3) account for 88.6 and 9.5% of variance, respectively.

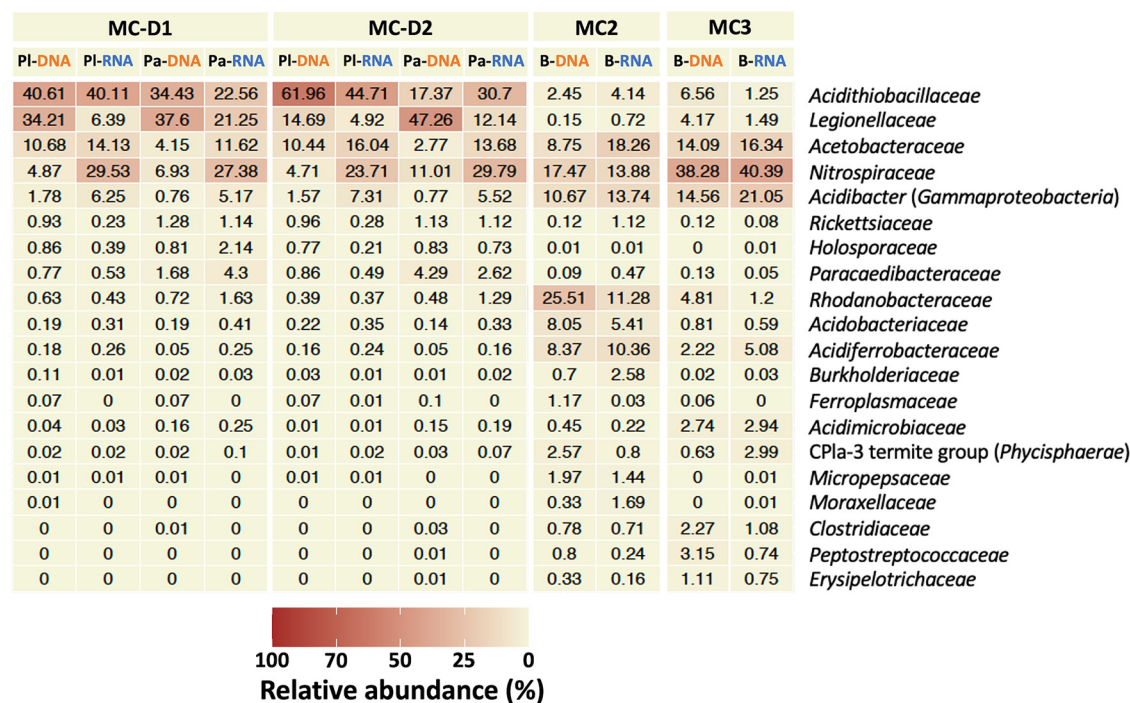| MC-D1				MC-D2				MC2		MC3		
Pl-DNA	Pl-RNA	Pa-DNA	Pa-RNA	Pl-DNA	Pl-RNA	Pa-DNA	Pa-RNA	B-DNA	B-RNA	B-DNA	B-RNA	
40.61	40.11	34.43	22.56	61.96	44.71	17.37	30.7	2.45	4.14	6.56	1.25	*Acidithiobacillaceae*
34.21	6.39	37.6	21.25	14.69	4.92	47.26	12.14	0.15	0.72	4.17	1.49	*Legionellaceae*
10.68	14.13	4.15	11.62	10.44	16.04	2.77	13.68	8.75	18.26	14.09	16.34	*Acetobacteraceae*
4.87	29.53	6.93	27.38	4.71	23.71	11.01	29.79	17.47	13.88	38.28	40.39	*Nitrospiraceae*
1.78	6.25	0.76	5.17	1.57	7.31	0.77	5.52	10.67	13.74	14.56	21.05	*Acidibacter* (*Gammaproteobacteria*)
0.93	0.23	1.28	1.14	0.96	0.28	1.13	1.12	0.12	1.12	0.12	0.08	*Rickettsiaceae*
0.86	0.39	0.81	2.14	0.77	0.21	0.83	0.73	0.01	0.01	0	0.01	*Holosporaceae*
0.77	0.53	1.68	4.3	0.86	0.49	4.29	2.62	0.09	0.47	0.13	0.05	*Paracaedibacteraceae*
0.63	0.43	0.72	1.63	0.39	0.37	0.48	1.29	25.51	11.28	4.81	1.2	*Rhodanobacteraceae*
0.19	0.31	0.19	0.41	0.22	0.35	0.14	0.33	8.05	5.41	0.81	0.59	*Acidobacteriaceae*
0.18	0.26	0.05	0.25	0.16	0.24	0.05	0.16	8.37	10.36	2.22	5.08	*Acidiferrobacteraceae*
0.11	0.01	0.02	0.03	0.03	0.01	0.01	0.02	0.7	2.58	0.02	0.03	*Burkholderiaceae*
0.07	0	0.07	0	0.07	0.01	0.1	0	1.17	0.03	0.06	0	*Ferroplasmaceae*
0.04	0.03	0.16	0.25	0.01	0.01	0.15	0.19	0.45	0.22	2.74	2.94	*Acidimicrobiaceae*
0.02	0.02	0.02	0.1	0.01	0.02	0.03	0.07	2.57	0.8	0.63	2.99	CPla-3 termite group (*Phycisphaerae*)
0.01	0.01	0.01	0	0.01	0.01	0	0	1.97	1.44	0	0.01	*Micropepsaceae*
0.01	0	0	0	0	0	0	0	0.33	1.69	0	0.01	*Moraxellaceae*
0	0	0.01	0	0	0	0.03	0	0.78	0.71	2.27	1.08	*Clostridiaceae*
0	0	0	0	0	0	0.01	0	0.8	0.24	3.15	0.74	*Peptostreptococcaceae*
0	0	0	0	0	0	0.01	0	0.33	0.16	1.11	0.75	*Erysipelotrichaceae*

100 70 50 25 0
Relative abundance (%)

FIG 3 Heat maps illustrating relative 16S rRNA (gene) sequence abundance (at the family level) of the present (DNA-based) and live (potentially active; RNA-based) microbial communities in planktonic (Pl), particle-associated (Pa), and benthic (B) fractions sampled in June 2017 at the middle course (MC) of the Rio Tinto during day 1 (MC-D1) and day 2 (MC-D2). Mineralogically heterogeneous sediment of the MC was subsampled (Fig. 1b). Relative abundances of specific taxa represent average values for triplicate samples of planktonic and particle-associated fractions and duplicate samples of benthic fractions, except for benthic samples collected from MC3, for which only one successful extraction was possible (Data Set S2). Heat maps were generated for taxa represented by more than 1% of relative sequence abundance.

nated in both DNA-based (38.3%, 14.1%, and 14.6%, respectively) and RNA-based (40.4%, 16.3%, and 21.1%, respectively) microbial communities (Fig. 3 and Data Set S2).

The microbial community of the water column at the upper estuary during low tide consisted of planktonic and particle-associated fractions dominated by *Rhodobacteraceae*, *Acetobacteraceae*, *Acidibacter*, and *Acidobacteriaceae* at DNA-based (9.1 to 30.6%, 25.5 to 45.5%, 5.2 to 13.7%, and 12.2 to 17.0%, respectively) and RNA-based (9.7 to 20.3%, 15.4 to 45.3%, 16.3 to 45.1%, and 8.0 to 9.0%, respectively) levels. During high tide, *Rhodobacteraceae* was the most dominant taxon of both the DNA-based (59.7%) and RNA-based (59.3%) planktonic microbial communities. The particle-associated DNA-based microbial community consisted mainly of *Acetobacteraceae* (26.9%) and *Rhodobacteraceae* (36.3%), while the RNA-based microbial community was dominated by *Acidihalobacteraceae* (13.3%), *Rhodobacteraceae* (29.5%), and *Acetobacteraceae* (28.7%) (Fig. 4 and Data Set S3).

The DNA-based benthic microbial communities of ES1 to ES3 were dominated by *Thermoplasmataceae* (7.5 to 30.9%), *Acidithiobacillaceae* (6.5 to 15.6%), and *Mariprofundaceae* (2.8 to 9.7%). For ES4, the DNA-based microbial community was dominated by unclassified *Thermoplasmataceae* (12.9%), while the RNA-based microbial community was dominated by unclassified *Desulfobacteraceae* (14.6%). ES-RP retrieved from sulfidic ES4 were dominated by *Thermoplasmataceae* (18.5%) at the DNA-based level and by *Thioalkalispiraceae* (9.8%) and *Desulfobacteraceae* (9.5%) at the RNA-based level. Beside marine microaerophilic Fe(II)-oxidizing *Mariprofundaceae*, freshwater *Gallionellaceae* and marine *Marinobacteraceae* were identified in the sediment. In addition, the benthic microbial community included the sulfate-reducing bacteria (SRB) *Syntrophobacteraceae* and *Desulfobulbaceae* as well as dissimilatory Fe(III)-reducing *Thermoanaerobaculaceae*, *Geobacteraceae*, and *Holophagaceae* (Fig. 4 and Data Set S3).

The Kruskal-Wallis test (52) with Benjamini-Hochberg correction (53) did not reveal any significances (adjusted P value, >0.05) when DNA- and RNA-based relative abundances of planktonic, particle-associated, and benthic microbial communities of the middle course and upper estuary of the Rio Tinto were compared (Data Set S5).
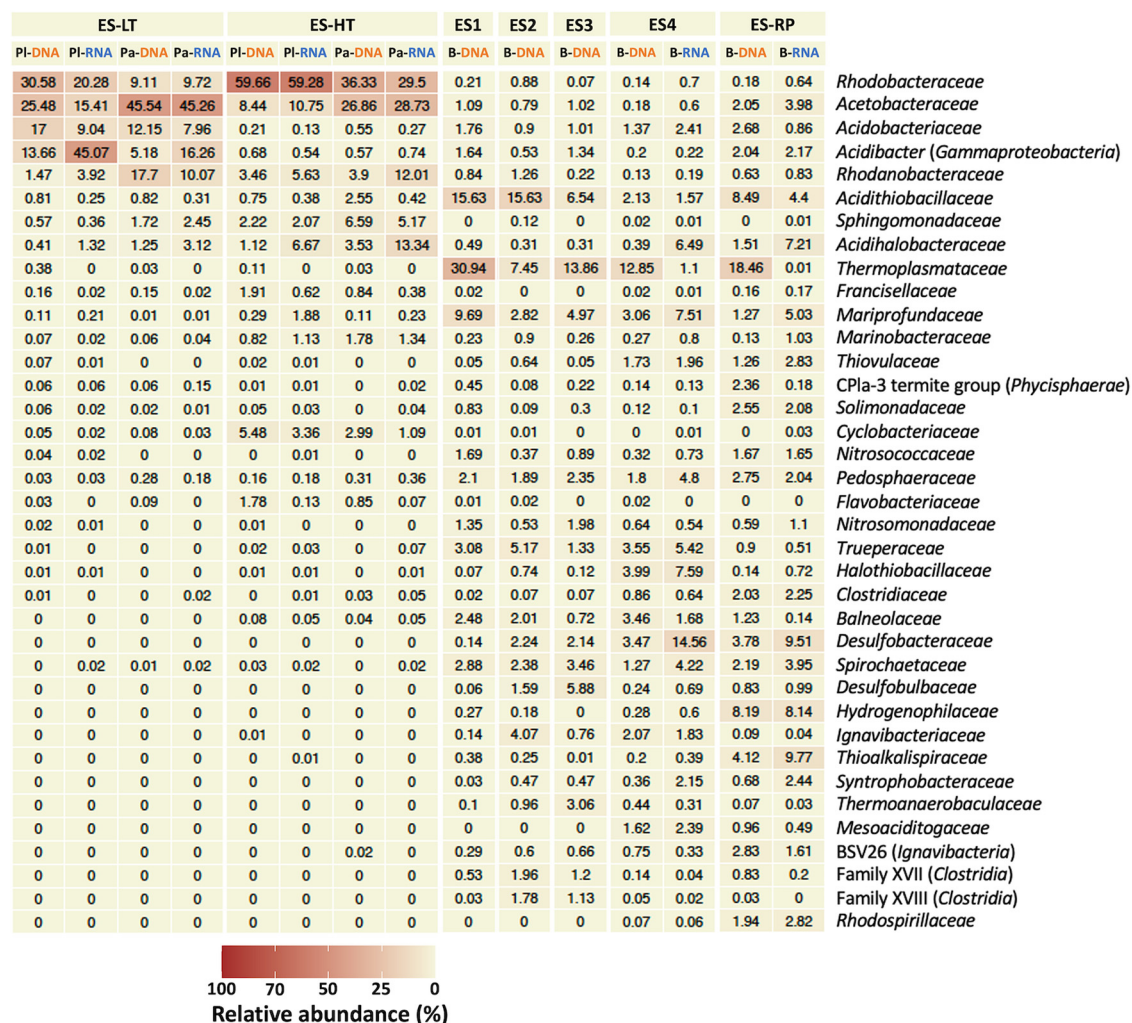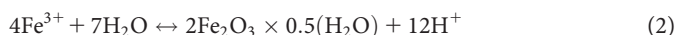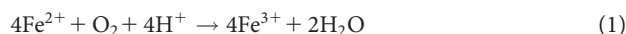
ES-LT Pl-DNA	ES-LT Pl-RNA	ES-LT Pa-DNA	ES-LT Pa-RNA	ES-HT Pl-DNA	ES-HT Pl-RNA	ES-HT Pa-DNA	ES-HT Pa-RNA	ES1 B-DNA	ES2 B-DNA	ES3 B-DNA	ES4 B-DNA	ES4 B-RNA	ES-RP B-DNA	ES-RP B-RNA	
30.58	20.28	9.11	9.72	59.66	59.28	36.33	29.5	0.21	0.88	0.07	0.14	0.7	0.18	0.64	Rhodobacteraceae
25.48	15.41	45.54	45.26	8.44	10.75	26.86	28.73	1.09	0.79	1.02	0.18	0.6	2.05	3.98	Acetobacteraceae
17	9.04	12.15	7.96	0.21	0.13	0.55	0.27	1.76	0.9	1.01	1.37	2.41	2.68	0.86	Acidobacteriaceae
13.66	45.07	5.18	16.26	0.68	0.54	0.57	0.74	1.64	0.53	1.34	0.2	0.22	2.04	2.17	Acidibacter (Gammaproteobacteria)
1.47	3.92	17.7	10.07	3.46	5.63	3.9	12.01	0.84	1.26	0.22	0.13	0.19	0.63	0.83	Rhodanobacteraceae
0.81	0.25	0.82	0.31	0.75	0.38	2.55	0.42	15.63	15.63	6.54	2.13	1.57	8.49	4.4	Acidithiobacillaceae
0.57	0.36	1.72	2.45	2.22	2.07	6.59	5.17	0	0.12	0	0.02	0.01	0	0.01	Sphingomonadaceae
0.41	1.32	1.25	3.12	1.12	6.67	3.53	13.34	0.49	0.31	0.31	0.39	6.49	1.51	7.21	Acidihalobacteraceae
0.38	0	0.03	0	0.11	0	0.03	0	30.94	7.45	13.86	12.85	1.1	18.46	0.01	Thermoplasmataceae
0.16	0.02	0.15	0.02	1.91	0.62	0.84	0.38	0.02	0	0	0.02	0.01	0.16	0.17	Francisellaceae
0.11	0.21	0.01	0.01	0.29	1.88	0.11	0.23	9.69	2.82	4.97	3.06	7.51	1.27	5.03	Mariprofundaceae
0.07	0.02	0.06	0.04	0.82	1.13	1.78	1.34	0.23	0.9	0.26	0.27	0.8	0.13	1.03	Marinobacteraceae
0.07	0.01	0	0	0.02	0.01	0	0	0.05	0.64	0.05	1.73	1.96	1.26	2.83	Thiovulaceae
0.06	0.06	0.06	0.15	0.01	0.01	0	0.02	0.45	0.08	0.22	0.14	0.13	2.36	0.18	CPla-3 termite group (Phycisphaerae)
0.06	0.02	0.02	0.01	0.05	0.03	0	0.04	0.83	0.09	0.3	0.12	0.1	2.55	2.08	Solimonadaceae
0.05	0.02	0.08	0.03	5.48	3.36	2.99	1.09	0.01	0.01	0	0	0.01	0	0.03	Cyclobacteriaceae
0.04	0.02	0	0	0	0.01	0	0	1.69	0.37	0.89	0.32	0.73	1.67	1.65	Nitrosococcaceae
0.03	0.03	0.28	0.18	0.16	0.18	0.31	0.36	2.1	1.89	2.35	1.8	4.8	2.75	2.04	Pedosphaeraceae
0.03	0	0.09	0	1.78	0.13	0.85	0.07	0.01	0.02	0	0.02	0	0	0	Flavobacteriaceae
0.02	0.01	0	0	0.01	0	0	0	1.35	0.53	1.98	0.64	0.54	0.59	1.1	Nitrosomonadaceae
0.01	0	0	0	0.02	0.03	0	0.07	3.08	5.17	1.33	3.55	5.42	0.9	0.51	Trueperaceae
0.01	0.01	0	0	0.01	0.01	0	0.01	0.07	0.74	0.12	3.99	7.59	0.14	0.72	Halothiobacillaceae
0.01	0	0	0.02	0	0.01	0.03	0.05	0.02	0.07	0.07	0.86	0.64	2.03	2.25	Clostridiaceae
0	0	0	0	0.08	0.05	0.04	0.05	2.48	2.01	0.72	3.46	1.68	1.23	0.14	Balneolaceae
0	0	0	0	0	0	0	0	0.14	2.24	2.14	3.47	14.56	3.78	9.51	Desulfobacteraceae
0	0.02	0.01	0.02	0.03	0.02	0	0.02	2.88	2.38	3.46	1.27	4.22	2.19	3.95	Spirochaetaceae
0	0	0	0	0	0	0	0	0.06	1.59	5.88	0.24	0.69	0.83	0.99	Desulfobulbaceae
0	0	0	0	0	0	0	0	0.27	0.18	0	0.28	0.6	8.19	8.14	Hydrogenophilaceae
0	0	0	0	0.01	0	0	0	0.14	4.07	0.76	2.07	1.83	0.09	0.04	Ignavibacteriaceae
0	0	0	0	0	0.01	0	0	0.38	0.25	0.01	0.2	0.39	4.12	9.77	Thioalkalispiraceae
0	0	0	0	0	0	0	0	0.03	0.47	0.47	0.36	2.15	0.68	2.44	Syntrophobacteraceae
0	0	0	0	0	0	0	0	0.1	0.96	3.06	0.44	0.31	0.07	0.03	Thermoanaerobaculaceae
0	0	0	0	0	0	0	0	0	0	0	1.62	2.39	0.96	0.49	Mesoaciditogaceae
0	0	0	0	0	0	0.02	0	0.29	0.6	0.66	0.75	0.33	2.83	1.61	BSV26 (Ignavibacteria)
0	0	0	0	0	0	0	0	0.53	1.96	1.2	0.14	0.04	0.83	0.2	Family XVII (Clostridia)
0	0	0	0	0	0	0	0	0.03	1.78	1.13	0.05	0.02	0.03	0	Family XVIII (Clostridia)
0	0	0	0	0	0	0	0	0	0	0	0.07	0.06	1.94	2.82	Rhodospirillaceae

100 70 50 25 0
Relative abundance (%)

FIG 4 Heat maps illustrating relative 16S rRNA (gene) sequence abundance (at the family level) of the present (DNA-based) and live (potentially active; RNA-based) microbial communities in planktonic (Pl), particle-associated (Pa), and benthic (B) fractions sampled in July 2017 at the upper estuary (ES) of the Rio Tinto during low tide (ES-LT) and high tide (ES-HT). Mineralogically heterogeneous sediment of the upper estuary was subsampled (Fig. 1b). Furthermore, red goethite-containing plaques (ES-RP) identified in the sulfidic sediment ES4 of the upper estuary were used for separate analysis. Microbial community analyses from layers ES1 to ES3 of the upper estuary sediment were DNA based only. Relative abundances of specific taxa represent average values for triplicate samples of planktonic and particle-associated fractions and duplicate samples of benthic fraction, except for benthic samples collected from ES1 and ES-RP, for which only one successful extraction was possible (Data Set S3). Heat maps were generated for taxa represented by more than 1.5% of relative sequence abundance.

DISCUSSION

Variations in water hydrogeochemistry at the middle course and upper estuary of the Rio Tinto. High levels of microbial Fe(II) oxidation (equation 1) at the middle course of the Rio Tinto lead to an oversaturation of the water with dissolved Fe(III), followed by precipitation of Fe(III) (oxyhydr)oxides (e.g., ferrihydrite) (equation 2) or hydroxysulfates (e.g., schwertmannite) (equation 3) (11, 12, 54).

$$4Fe^{2+} + O_2 + 4H^+ \rightarrow 4Fe^{3+} + 2H_2O \qquad (1)$$

$$4Fe^{3+} + 7H_2O \leftrightarrow 2Fe_2O_3 \times 0.5(H_2O) + 12H^+ \qquad (2)$$

$$16Fe^{3+} + 2SO_4{}^{2-} + 28H_2O \rightarrow Fe_{16}O_{16}(OH)_{12}(SO_4)_2 + 44H^+ \qquad (3)$$

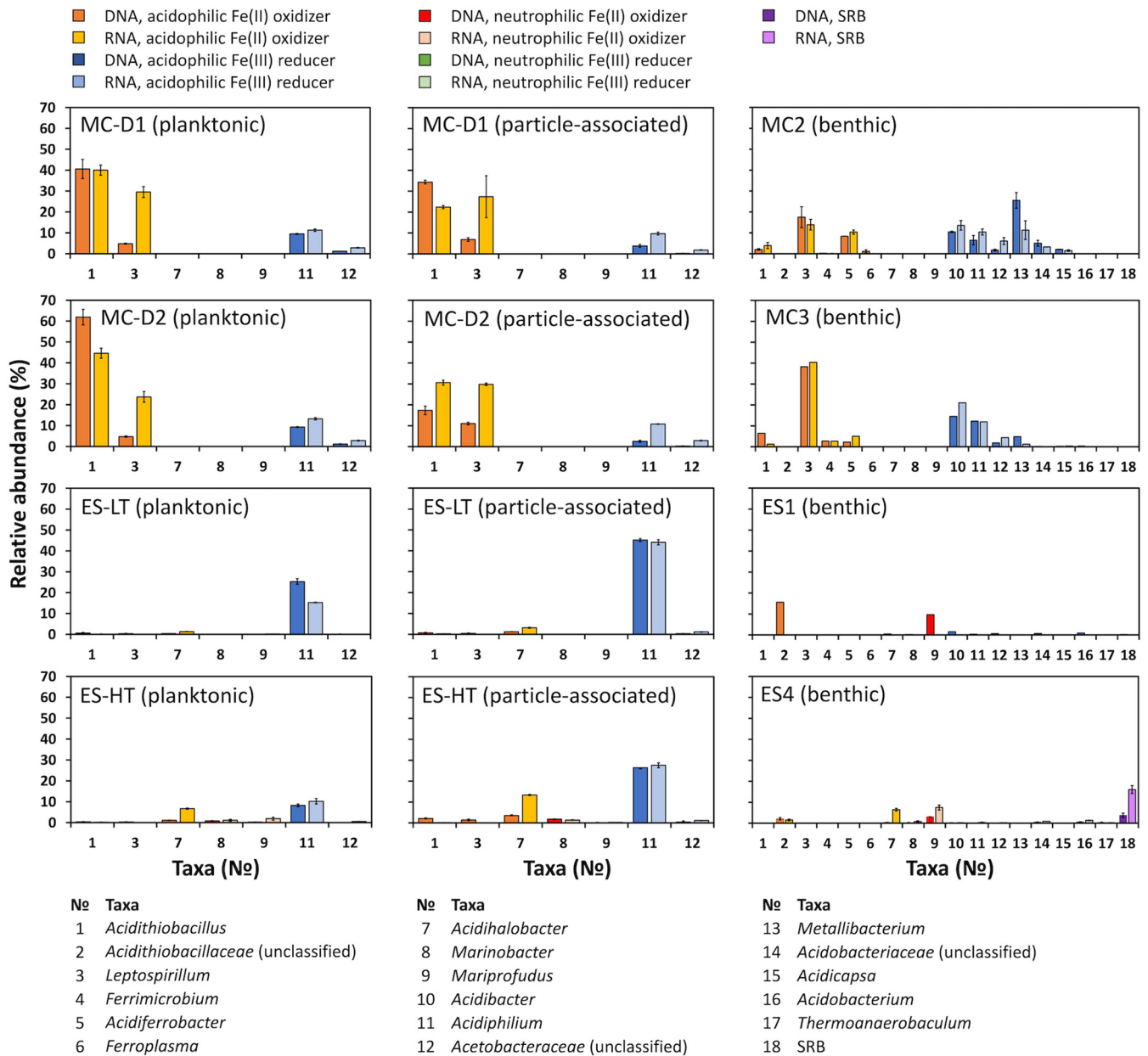This Fe buffering system consumes OH^- groups, releases H^+, and maintains the low

FIG 5 Relative 16S rRNA (gene) sequence abundance (at the genus level) of the present (DNA-based) and alive (potentially active; RNA-based) Fe-cycling microbial community in planktonic, particle-associated, and benthic fractions sampled at the middle course (MC) and at the upper estuary (ES) of the Rio Tinto in June/July 2017. Planktonic and particle-associated fractions of the water from the MC and the ES were sampled at two time points. At the middle course, samples were collected at two consecutive days (MC-D1 and MC-D2). At the upper estuary, samples were collected during low (ES-LT) and high tide (ES-HT) during the same day. Mineralogically heterogeneous sediments of the middle course and the upper estuary were subsampled (Fig. 1b). Microbial community analysis from ES1 of the upper estuary sediment were DNA based only. Results of analysis of samples ES2, ES3, and ES-RP are reported in Fig. S6. Relative abundances of specific taxa represent average values for triplicate samples of planktonic and particle-associated fractions and duplicate samples of benthic fractions, except for benthic samples collected from MC3 and ES1, for which only one successful extraction was possible (Data Set S4). SRB data summarize the relative abundance of unclassified *Desulfobacteraceae*, unclassified *Desulfobulbaceae*, *Desulfonatronobacter*, and *Syntrophobacter*.

pH values that were observed at the middle course over 2 days (11, 12, 54). The slight increase in pH at the upper estuary compared to the middle course was caused by pH-neutral tidal water, entering the estuary (Table 1). In our previous study, we calculated that the proportion of seawater at the upper estuary during sampling varied from 34% to 83% at low and high tide, respectively (21). Nevertheless, the pH remained comparatively low due to precipitation of dissolved Fe(III) and other solutes (e.g., Al, Cu, etc.) with Cl^-, SO_4^{2-}, OH^-, and other anions (Table 1) as copper ferrite, Fe(III) dihydroxochloride, F (III) hydroxide, goethite, hematite, jarosite, magnetite, alunite, jurbanite, maghemite, nsutite,

and pyrolusite (Data Set S6). Precipitation of dissolved Fe(III) at the upper estuary led to a progressive decrease of dissolved Fe(III) to 6.6 mg/L (low tide) and 2.9 mg/L (high tide) (Table 1), followed by a decrease in Fe buffer capacity (13). However, the buffer capacity was still sufficient to maintain the low pH, which played a key role in preventing abiotic oxidation of Fe(II) at the upper estuary (55). Thus, in contrast with Fe(III), the estuarine Fe(II) content remained comparatively high and varied from 9.4 mg/L (low tide) to 2.8 mg/L (high tide). Collectively, these results suggest that the estuarine water may harbor acidophilic Fe-cycling microorganisms. However, the high Cl^- concentrations might have a negative or even inhibiting effect on such microorganisms, due to their positively charged membrane that facilitates the influx of permeable anions. It has been shown before that the influx of Cl^- into cells of acidophilic microorganisms can cause the collapse of membrane potentials and the proton motive force, as well as a general poisoning of the cytoplasm (45, 56).

For the different sampling events, principal-component analysis (PCA) was used to visualize the key hydrogeochemical parameters, including the values of salinity, E_h, and pH as well as concentrations of NO_3^-, SO_4^{2-}, Fe(III), Fe(II), O_2, Na^+, and Cl^- (Fig. 2f). The PCA delineated the separation of three hydrogeochemical conditions at the middle course and the upper estuary of the river. At the middle course, the hydrogeochemistry of the water was remarkably stable over 2 days, while at the upper estuary during low and high tide, it changed substantially. Therefore, we further discuss the *in situ* processes that affect the fate of Cr, As, Pb, and Cd in the distinguished hydrogeochemical zones.

At the middle course over 2 days, the low pH kept As and Cd (>99%) predominantly dissolved in the water, while 14 to 21% of Pb and 16 to 22% of Cr were identified in the SPM-associated fraction (Fig. 2a and c). The precipitation of HMs, especially prominent for Pb and Cr above others, was induced by microbial oxidation of Fe(II) (57). Part of the poorly crystalline, low-density Fe(III) minerals, produced by microbial Fe(II) oxidation, remain suspended in the water even over long periods of time and can be then transported to the river estuary (21, 44).

In the upper estuary water column, mixing events lead to neutralization and the progressive loss of dissolved sulfate via the precipitation of sulfated salts (e.g., alunite, jarosite, and jurbanite) (Data Set S6). The precipitating sulfates scavenge an important fraction of some dissolved HMs that have been transported downriver. Furthermore, the neutralization of the river water leads to the formation of colloidal Fe(III) hydroxides [e.g., Fe(III) dihydroxochloride, Fe(III) hydroxide etc.] (Data Set S6) that coprecipitate HMs (58–60). The lower concentrations of dissolved Cr, As, and Cd in the upper estuary compared to the middle course suggests that these precipitation events systematically remove HMs. In contrast, the concentration of Pb slightly increased in the upper estuary (Fig. 2b), which is likely due to the dissolution of Pb sulfates (e.g., anglesite) in the presence of elevated Cl^- concentrations (21, 61, 62). The same process could lead to a decrease of SPM-associated Pb in the estuarine water (Fig. 2d). SPM-associated fractions of Cr and especially As remained high, despite the dilution of river water with seawater. These metals, particularly As, are strongly sorbed and/or coprecipitated on/with oxyhydroxysulfates (13). Although precipitation of solutes in the upper estuary obviously increased the content of SPM (Fig. 2e), it should be noted here that this fraction can also contain particles (including microbial cells) that are transported to the upper estuary with the inflowing tidal water.

Key microbial players involved in Fe redox transformation under acidic conditions at the middle course. The Rio Tinto maintains two divergent but interrelated transport pathways of SPM, which consists not only of minerals but also of planktonic and particle-associated microbial cells. The longitudinal pathway provides a constant source of SPM into the river estuary, while the sedimentation pathway provides a constant burial of SPM in the sediment throughout the river. The results of PCA clearly distinguished three hydrogeochemical conditions, forming at the middle course of the river, at the upper estuary during low tide and at the upper estuary during high tide (Fig. 2f). Therefore, suspended cells transported by the longitudinal pathway might pass through at least three different hydrogeochemical conditions. Furthermore, the sedimentation of SPM constantly transports microbial cells from the water column into the river sediment (44, 63). The spatial and temporal hydrogeochemical changes forming along the river can have a noticeable effect on

activity and distribution of microorganisms. The comparison of the DNA- and RNA-based relative abundance profiles helped to distinguish between the present (dead or extracellular DNA) and live (potentially active) Fe-cycling cells (48–51, 64, 65). Although the Kruskal-Wallis test (52) with Benjamini-Hochberg correction (BH) (53) did not reveal any significant differences below the 0.05 threshold between DNA- and RNA-based relative abundances of planktonic, particle-associated, and benthic microbial communities of the middle course and the upper estuary of the Rio Tinto, many taxa were different when a BH-corrected P value threshold of 0.11 was used (Data Set S5). Furthermore, in many cases the hydrochemistry can be used to explain the observed differences between the present (DNA level) and potential active (RNA level) microbial communities.

The consistently acidic water of the middle course, characterized by a high concentration of dissolved Fe(II) and oversaturation of Fe(III), was predominantly inhabited by Fe(II)-oxidizing *Acidithiobacillus* (family *Acidithiobacillaceae*) and *Leptospirillum* (family *Nitrospiraceae*) (Fig. 5). Both taxa are typically resistant to high E_h values. However, members of the genus *Leptospirillum* may outcompete other acidophilic Fe(II)-oxidizing microorganisms due to their greater affinity for Fe(II) and greater tolerance to oxidative stress, caused by high concentration of dissolved Fe(III) (66, 67). While the DNA-based community composition stipulates that *Acidithiobacillus* was the main driver of Fe(II) oxidation in the planktonic and particle-associated fractions, the RNA-based relative abundance demonstrates that both *Acidithiobacillus* and *Leptospirillum* were almost equally abundant and, therefore, potentially active in the planktonic and particle-associated microbial communities (Fig. 5). The higher RNA/DNA relative abundance ratio suggests *Leptospirillum* as the most metabolically active Fe(II)-oxidizing taxon at the middle course. Indeed, *Leptospirillum* has been shown to resist reactive oxygen species (ROS) more efficiently than *Acidithiobacillus* (66, 67). In contrast to *Acidithiobacillus*, the antioxidant protection system of *Leptospirillum* is focused on repairing the cellular damage rather than on degrading ROS (66, 67). Thus, at higher Fe(III)/Fe(II) ratios, *Leptospirillum* might more efficiently couple Fe(II) oxidation with O_2 reduction (68, 69).

For the same reason, *Leptospirillum* might gain a competitive advantage in putative microoxic benthic environments of the middle course, where they dominated over other Fe(II)-oxidizing taxa at both DNA- and RNA-based levels (Fig. 5). Furthermore, under the O_2-limited conditions, *Leptospirillum* might express terminal oxidases, allowing this organism to adapt to low oxygen levels (70). In the microoxic sediment, we also identified a high DNA- and RNA-based relative abundance of Fe(II)-oxidizing *Acidiferrobacter* (family *Acidiferrobacteraceae*). The diversity and taxonomy of *Acidiferrobacter* remains poorly constrained. However, its presence in many habitats suggests that this taxon has an important ecological role and supports the need for further studies (71). This taxon, as well as some other identified Fe(II) oxidizers, is able to couple the oxidation of reduced sulfur species or H_2 to Fe(III) reduction in anoxic environments (72).

The high content of dissolved and particulate Fe(III) in the water column of the middle course might maintain the activity of heterotrophic members of the phylum *Proteobacteria*, such as those belonging to the genera *Acidibacter* and *Acidiphilium* (family *Acetobacteraceae*) as well as to unclassified members of the family *Acetobacteraceae*. These findings corroborate previous microbial diversity studies of the Rio Tinto, although *Acidibacter* has typically been reported to be more abundant than *Acidiphilium* (32, 33). However, only *Acidiphilium* was shown to respire Fe(III) in the presence of oxygen in the water column (73, 74) while *Acidibacter* is most likely capable of catalyzing reductive dissolution of the Fe(III) only under microoxic and anoxic conditions (36, 75–77). Nevertheless, both identified heterotrophs likely consume organic matter in the oxygenated water column. When only the DNA-based relative abundances of *Acidiphilium* and unclassified *Acetobacteraceae* in planktonic and particle-associated microbial communities are considered, the dominance of Fe(III)-reducing taxa might be misrepresented. Comparing RNA-based relative abundances in the water column over 2 days, we concluded that *Acidiphilium* organisms were likely alive and had similar relative abundances (Fig. 5). The *Acidiphilium* and unclassified *Acetobacteraceae* identified in the water column as well as several other taxa known as acidophilic Fe(III) reducers dominated in RNA-based microbial communities in sediments MC2 and MC3, where, under putative

microoxic conditions, they could couple organic matter oxidation with O_2 or Fe(III) respiration (35–37, 75–77). Indeed, we observed an increase in the DNA- and RNA-based relative abundances of unclassified *Acetobacteraceae* and *Acidibacter* [putative anoxic Fe(III) reducers] compared to Fe(II)-oxidizing microorganisms. The microoxic sediments with potential anoxic niches and high availability of carbon sources likely provide them with a competitive advantage over Fe(II) oxidizers. In contrast to other heterotrophs, the Fe(III)-reducing *Metallibacterium* (family *Rhodanobacteraceae*) was more abundant according to DNA analysis than RNA analysis. This observation suggests that the DNA-based approach alone might overestimate the potential activity of *Metallibacterium* in the sediment of the middle course (Fig. 5).

In summary, the hydrogeochemistry of the water column at the middle course favored the presence of *Leptospirillum*, *Acidithiobacillus* and *Acidiphilium*. These taxa were potentially active in planktonic and particle-associated fractions. In turn, they probably shaped the hydrogeochemistry of the river at the middle course. Fe(III) reducers consumed organic matter (e.g., acetate) which might inhibit the growth of acidophilic Fe(II)-oxidizing autotrophs and the recycling of Fe(II), while Fe(II) oxidizers produced dissolved Fe(III), which is required to maintain the low water pH (equations 1 to 3). In sediments MC2 and MC3 of the middle course, *Leptospirillum*, *Acidiferrobacter*, *Acidithiobacillus*, and *Ferrimicrobium* were likely the key Fe(II) oxidizers, while *Acidiphilium*, *Acidibacter*, *Metallibacterium*, and *Acidicapsa* were probably the main Fe(III) reducers (Fig. 5).

Abundance and activity of the Fe-cycling microbial community under the dynamic conditions of the upper estuary. The pronounced decline of the DNA-based and, especially, RNA-based relative abundances of *Acidithiobacillus* and *Leptospirillum* with respect to other members of the estuarine microbial community (Fig. 5) suggests that, despite the low pH and available Fe(II), the elevated concentration of Cl^- in the water inhibits the potential activity of Fe(II) oxidizers that thrive at the middle course of the river (45, 56). Nevertheless, the unique combination of hydrogeochemical parameters in the upper estuary favored the increase in relative abundance of potentially active marine neutrophilic *Mariprofundus* (family *Mariprofundaceae*) and *Marinobacter* (family *Marinobacteraceae*), as well as the acidophilic and halotolerant *Acidihalobacter* (family *Acidihalobacteraceae*). The microaerophilic *Marinobacter* was almost equally relatively abundant at DNA- and RNA-based levels in the planktonic and particle-associated microbial communities during high tide, while the RNA-based relative abundances of *Mariprofundus* were >1% only in the high-tide planktonic microbial community. Nevertheless, the RNA-based relative abundance of *Mariprofundus* was higher than the DNA-based one, indicating a potentially higher activity level of these planktonic cells in the estuarine water (Fig. 5).

As a consequence of the low pH and high salinity, *Acidihalobacter* was the only abundant Fe(II) oxidizer (RNA-based analysis) in the planktonic and particle-associated microbial communities during low tide. Notably, the DNA-based relative abundance of *Acidihalobacter* might underestimate the role of this taxon. This conclusion is particularly obvious when the DNA-based relative abundances of *Acidihalobacter*, *Leptospirillum*, and *Acidithiobacillus* in the particle-associated microbial community of the water, sampled during high tide, are compared (Fig. 5).

Surprisingly, despite the high salinity, acidophilic heterotrophs affiliating with the families *Acetobacteraceae* (e.g., *Acidiphilium*), *Acidibacter* and *Acidobacteriaceae* (e.g., *Acidobacterium*) dominated in the low-tide water (Fig. 4). However, only *Acidiphilium* is known to couple the oxidation of organic matter with Fe(III) reduction in the oxygenated water column (Fig. 5). In contrast to the middle course, the estuarine sediment is rich in organic matter (44, 63) which might be resuspended from the sediment or produced by microalgae thriving in the estuary. Comparative analyses of the DNA- and RNA-based relative abundances demonstrated that *Acidibacter* dominated in the fraction of active microorganisms during low tide, in particularly in the planktonic microbial community (Fig. 4). Conversely, during high tide, mainly *Acidiphilium* (family *Acetobacteraceae*) remained potentially active (Fig. 5), due to its higher tolerance to Cl^- compared to many other acidophiles (78, 79). The precipitation of solutes, the SPM transported by the river, and the sandy sediment transported by the tidal water as well as seasonal and annual variation in tidal activity and river flow contributed to the

formation of a massive sediment layer at the upper estuary. As previously reported, the estuarine sediment was enriched with organic matter (7.9 to 14.2% [by weight]), Fe(III) minerals (e.g., schwertmannite, ferrihydrite, and goethite), and Fe(II) sulfides (21, 44, 63, 80). The RNA was extracted only from sediment ES4 and from goethite-containing ES-RP retrieved from ES4 (Fig. 1b). The high content of organic matter, reducing conditions, and available sulfate likely stimulated the growth of sulfate-reducing members of the class *Deltaproteobacteria*, such as those belonging to the taxa *Desulfobacteraceae*, *Desulfobulbaceae*, and *Syntrophobacter* (family *Syntrophobacteraceae*) (Fig. 5). The decrease of Fe(III) concentrations in the estuary water and the high content of Fe sulfides in the sediments demonstrates that SRB might play an important role in Fe sequestration (63). These microorganisms may lead to the indirect reductive dissolution of Fe(III) minerals with H_2S (81), which leads to the formation of secondary minerals, including vivianite or Fe(II)-containing sulfides (e.g., mackinawite, pyrite, or greigite) (82, 83). In addition, SRB can use solid-phase sulfate in Fe(III) hydroxysulfates as a direct electron acceptor (83). The higher RNA-based relative abundances of these microorganisms in ES4 suggested that SRB were alive and metabolically active in the sediment. The consumption of H^+ during sulfate reduction and the subsequent reaction of its by-product, H_2S, with Fe(III) minerals might contribute to a pH increase, E_h decrease, and accumulation of Fe(II) sulfides (84).

Fe(II) sulfides, as well as dissolved Fe(II), might be used as electron donors by the Fe(II)-oxidizing, neutrophilic (*Mariprofundus* and unclassified *Gallionellaceae*), and acidophilic (*Acidihalobacter* and unclassified *Acidithiobacillaceae*) taxa. Additionally, under anoxic conditions, *Acidihalobacter* and unclassified *Acidithiobacillaceae* might couple the oxidation of sulfur species with Fe(III) reduction. Abundant Fe(III) minerals could be also reduced by neutrophilic *Thermoanaerobaculum* (family *Thermoanaerobaculaceae*), *Geobacter* (family *Geobacteraceae*), and *Geothrix* (family *Holophagaceae*), acidophilic *Acidibacter*, *Acidobacterium*, *Acidiphilium*, and unclassified *Acetobacteraceae* under anoxic conditions. The comparative analysis of DNA- and RNA-based relative abundances of *Mariprofundus*, *Marinobacter*, and *Acidihalobacter* indicated that these taxa were potentially active in the Fe(II)-rich sediment ES4 and in the red goethite-containing plaques retrieved from this layer. We also found that unclassified *Acidithiobacillaceae* was abundant in the DNA-based microbial community. However, the RNA-based analysis demonstrated that, at least in sediment ES4, this taxon was less abundant and potentially less active compared to *Acidihalobacter* and *Mariprofundus* (Fig. 5).

Analysis of DNA- and RNA-based relative abundances revealed distinct differences in the Fe-cycling microbial communities of the middle course and the upper estuary. Considering the RNA-based relative abundance as a potential indicator of microbial activity, we found that at the Fe(III)-rich middle course, *Acidithiobacillus* and *Leptospirillum* were the most abundant and potentially active taxa in planktonic and particle-associated fractions. Conversely, at the upper estuary, daily pH and Cl^- fluctuations, high salinity, comparatively low Fe(III), and comparatively high Fe(II) contents likely contributed to the increase in RNA-based abundance of *Acidihalobacter*. During high tide, we observed an increase of RNA-based relative abundances of *Marinobacter* and *Mariprofundus*, which likely act as the main drivers of Fe(II) oxidation at the upper estuary. *Acidiphilium* was identified as an Fe(III) reducer at both field sites. *Acidibacter* and *Acidobacterium* (family *Acidobacteriaceae*), which dominated in the estuary, probably do not play an important role in Fe(III) reduction due to the high content of O_2. Fe(II) oxidation at the middle course sediment was potentially predominantly performed by acidophilic microorganisms, while at the upper estuary, *Marinobacter* and *Mariprofundus* might also contribute to Fe(II) oxidation. Fe(III) reduction in the sediment of the upper estuary might be performed by SRB that were abundant at the RNA-based level (Fig. 6). Thus, our data suggest that Fe cycling in the estuarine sediment is not only driven by acidophilic microorganisms but also by the typically neutrophilic Fe(II)-oxidizing *Marinobacter*, *Mariprofundus*, and unclassified *Gallionellaceae* as well as by the neutrophilic Fe(III)-reducing *Thermoanaerobaculum*, *Geobacter*, *Geothrix*, and SRB. The differences between the DNA- and RNA-based 16S rRNA (gene) sequencing profiles of planktonic, particle-associated, and benthic microbial communities indicated that complementary methodological approaches should be applied to identify present and potentially active Fe-cycling microorganisms.
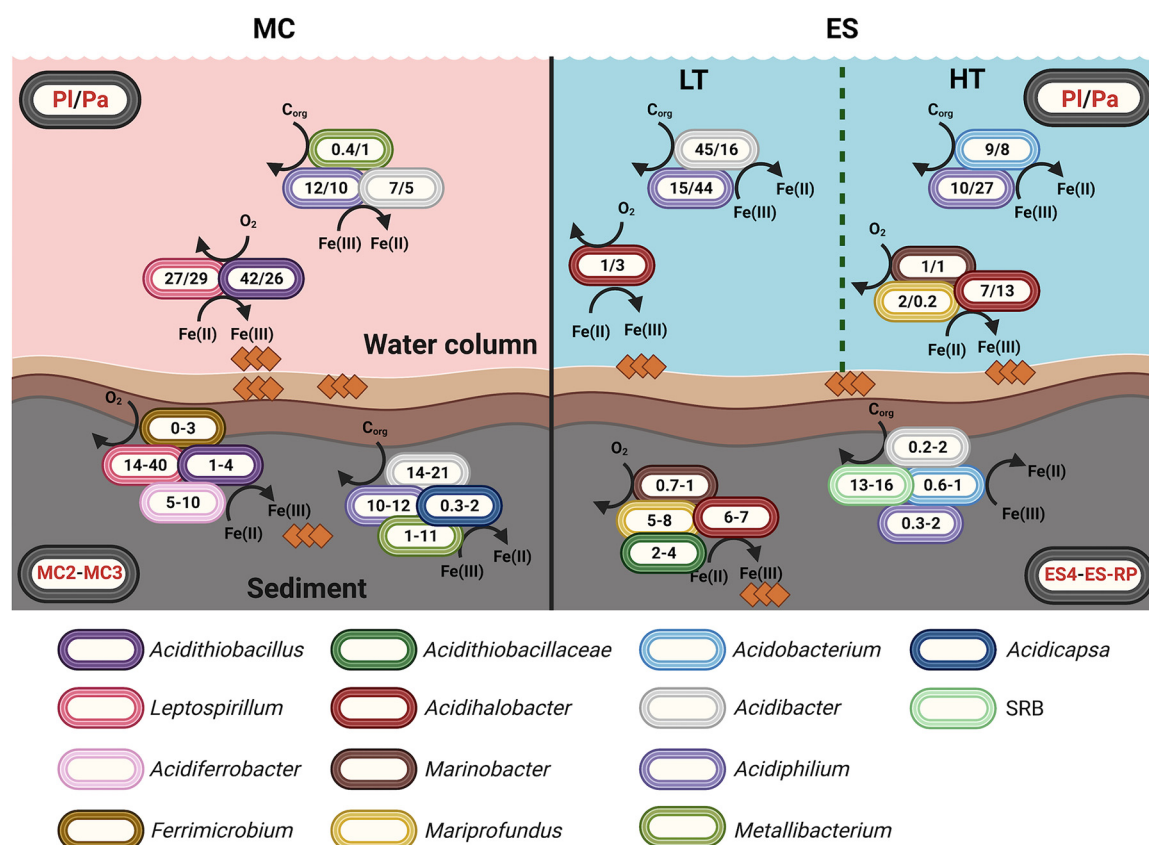
FIG 6 Microbial taxa involved in Fe cycling at the middle course and the upper estuary of the Rio Tinto. Relative abundance (at the genus level) of the live (potentially active; RNA-based) taxa predominant in planktonic (Pl), particle-associated (Pa), and benthic fractions sampled at the middle course (MC) and at the upper estuary (ES) of the Rio Tinto during low tide (LT) and high tide (HT) in June/July 2017. Relative abundances of Pl and Pa taxa at the middle course represent average values of relative abundances identified over 2 days of sampling (created with BioRender.com).

Impact of microbially induced Fe redox transformations on the mobility of As, Cr, Cd, and Pb at the middle course and upper estuary of the Rio Tinto. The precipitation of Fe(III) minerals at the cell surface might be accompanied by the coprecipitation of dissolved HMs, including As, Cr, Cd, and Pb, at the middle course of the river (13, 21, 85). Produced cell-mineral aggregates with coprecipitated HMs could remain suspended in the water column and therefore replenish the SPM pool. The SPM is transported to the upper estuary by the longitudinal pathway (29). However, the progressive aggregation of SPM leads to the formation of dense and heavy particles which settle to the riverbed and enrich the sediment with Fe(III) minerals, coprecipitated HMs, organic matter, and living microorganisms. At the sediment of the middle course, intensive aerobic respiration leads to the depletion of O_2 (86). The subsequent formation of microoxic or anoxic conditions favors anaerobic respiration, for example reduction of Fe(III) minerals coupled either to the oxidation of organic matter by *Acidiphilium* and *Acidibacter* or to the oxidation of reduced sulfur compounds by *Acidithiobacillus and Acidiferrobacter* (37, 87). Finally, the reductive dissolution of Fe(III) minerals may lead to a partial recycling of Fe(II) to the water column and to the remobilization of As, Pb, Cr, Cd and other HMs.

The fate of HMs at the upper estuary of the Rio Tinto is poorly understood, since the processes affecting HM behavior are often difficult to separate. The effects of the physicochemical processes occurring in the water column can overlap the effects of biological activity or input of material from the underlying sediment (40, 88). Nevertheless, it is well known that the inflow of seawater results in the precipitation of solutes predominantly as sulfates, which can scavenge a large portion of the dissolved HMs, predominantly Cr and As transported by the river water (13, 14, 20, 44, 58, 59). The formation of amorphous

particulate matter that has a developed surface area could contribute to the removal of other metals by absorption (e.g., Pb and Zn). This abiotic process likely removes a large portion of HMs from the dissolved state. However, the immobilization of HMs can be also induced by microbial Fe(II) oxidation and the subsequent precipitation of Fe(III) minerals in acidic estuarine water. In these environments, the oxidizing part of the Fe cycle could be operated by acidophilic and halotolerant *Acidihalobacter* (during low tide and high tide) or even by marine neutrophilic *Mariprofundus* and *Marinobacter* (during high tide), which typically require microaerophilic conditions to outcompete abiotic Fe(II) oxidation.

Predominantly abiotic precipitation of HMs in the estuarine water would lead to a progressive rise of the SPM-associated fraction of HMs (Fig. 2d). Therefore, the degree to which HMs are transported in their particulate form, and how those particles behave, is an important driver of their fate in the estuary (21, 59, 89). Part of the low-density particulate matter will not settle out of the water column even over long periods of time because their gravitational settling rate is less than their random displacement by the Brownian motion of the surrounding water molecules (44). However, part of the immobilized HMs in the particulate matter could be removed from the water column by sedimentation into the upper sediment layer of the estuary. The subsequent reduction of Fe(III) minerals indirectly by SRB could facilitate the retention of HMs in the form of sulfides or contribute to their immobilization with Fe(II) sulfides (21, 90). In contrast, Fe(III)-reducing neutrophilic *Thermoanaerobaculum*, *Geobacter*, and *Geothrix* could accelerate the reductive dissolution of Fe(III) minerals and diffusion of mobilized HMs back to the water column.

Thus, the different hydrogeochemical environments formed at the middle course and in the upper estuary of the Rio Tinto likely shape the composition of the Fe-cycling microbial community and their activity in relation to Fe. In turn, redox transformation of Fe directly affects the state and mobility of HMs such as, e.g., Cr, As, Cd, and Pb.

MATERIALS AND METHODS

Field sites and sampling procedure. Samples were collected from the Rio Tinto middle course (near Berrocal village; 37.593727 N, 6.551104 W) and upper estuary (under the bridge in San Juan del Puerto; 37.311194 N, 6.822889 W) during the dry season (29 June 2017 to 02 July 2017) (Fig. 1a). River water was sampled from a 30-cm depth in triplicate every 2 h for 2 days at the middle course and for 1 day at the upper estuary (Fig. 1b). During the sampling event directly in the field, 2 L of water at the middle course and 1 L at the upper estuary were prefiltered with 0.45-μm-pore-size membrane filter (HAWG050S6; Merck). Filtered water (45 mL) was stabilized with 5 mL of 10% HNO_3 (for analysis; Merck) and stored in the dark at 4°C for the HM analysis. Filtered water (50 mL) for quantification of anions was stored in the dark at 4°C prior to analysis. Representative samples of sediment were collected from the bank of the river at both sites and stored in tightly closed plastic containers in the dark at room temperature until mineralogical and elemental analysis. Temperature, pH, salinity, and oxygen content of the water were determined *in situ* at both sites over 2 days at the middle course and during 1 day at the upper estuary with 2-h intervals using a field multimeter (WTW; Multi 3430). The multimeter was equipped with a pH electrode with a temperature sensor (WTW; SenTrix), a conductivity electrode (WTW; TetraCon92) and an O_2 sensor (WTW; FDO925). The redox potential was determined using a pH meter (Mettler-Toledo; SG2) with Pt and Ag/AgCl electrodes. We used PCA to assess the variability of hydrochemical parameters at the middle and at the upper estuary. The hydrochemical data are available in Table 1. PCA was performed using hydrogeochemical parameters with correlation coefficients calculated using R, version 3.6.2, in the tidyr package (91).

For the collection of planktonic and particle-associated biomass samples, we separately collected triplicate samples of river water (2 L each) (Fig. 1b). The river water was collected twice at the middle course (29 June 2017, 16:00, and 30 June 2017, 16:00) and twice at the upper estuary during low (02 July 2017, 0:00) and high (02 July 2017, 6:00) tides. Then, water samples were filtered through 8-μm (SCWP04700; Merck) and 0.22-μm (GSWG047S6; Merck) mixed-cellulose-ester (MCE) filters directly on site. All filters were placed in sterile 2-mL centrifuge tubes and stored immediately at −20°C for later DNA and RNA extraction. For sampling benthic biomass, we retrieved duplicate sediment cores and collected three sediment layers from the depth 0.0 to 0.5 cm (MC1), 0.5 to 1.0 cm (MC2), and 1.0 to 1.5 cm (MC3) at the middle course. At the upper estuary, we collected duplicate samples of sediment from the following depths: 0.0 to 1.5 cm (ES1), 1.5 to 3.0 cm (ES2), 3.0 to 4.5 cm (ES3), and 4.5 to 6.0 cm (ES4) of the littoral zone during low tide. In addition, we specifically sampled red plaques (ES-RP), which are especially abundant in the sulfidic part of the ES4 (Fig. 1b). All sediment samples were placed in sterile 15-mL centrifuge tubes and stored immediately at −20°C for DNA and RNA extraction.

DNA and RNA extraction, DNA digestion, reverse transcription, amplification, and sequencing. Total DNA and RNA were extracted separately from 8-μm (particle-associated) and 0.22-μm (planktonic) membrane filters (triplicate samples for each time point) and sediment samples (duplicate samples for each layer) as described by Lueders et al. (92). Aliquots of DNA and RNA coextracts (5 μl) were used for DNA digestion with the Ambion Turbo DNA-free kit, as directed by the manufacturer (Life Technologies, Carlsbad, CA, USA). Afterward, reverse transcription reactions were performed using a reverse transcriptase (SuperScript III) to generate cDNA, as described by the manufacturer. The 16S

rRNA (gene) (DNA and cDNA) was amplified using primers 515F and 806R targeting the V4 region (93). Subsequent library preparation steps (Nextera, Illumina) and 250-bp paired-end sequencing with MiSeq (Illumina, San Diego, CA, USA) using v2 chemistry were performed by Microsynth AG (Switzerland), and between 55,862 and 170,160 read pairs (average, 114,928 read pairs) were obtained for each sample in two separate sequencing runs on the same MiSeq machine. Quality control, reconstruction of 16S rRNA (gene) sequences, and taxonomic annotation was performed with nf-core/ampliseq v1.1.0 (10.5281/zenodo.2244493) (94, 95) with Nextflow v20.10.0 (96) and singularity v3.4.2 (97). Data from the two sequencing runs were treated initially separately by the pipeline using the option "–multipleSequencingRuns," and ASV tables were merged. Primers were trimmed and untrimmed sequences were discarded (<4%) with Cutadapt v1.16 (98). Adapter and primer-free sequences were imported into QIIME2 v2018.06 (99), their quality was checked with demux (https://github.com/qiime2/q2-demux), and they were processed with DADA2 (100) to remove PhiX contamination, trim reads (before median quality drops below 35, that is, forward 181 and reverse 163), correct errors, merge read pairs, and remove PCR chimeras; ultimately, 3,497 amplicon sequencing variants (ASVs) were obtained across all samples. Alpha rarefaction curves were produced with the QIIME2 diversity alpha-rarefaction plug-in, which indicated that the richness of the samples had been fully observed. Rarefaction curves can be found in the Fig.S7 and S8. A naive Bayes classifier was fitted with 16S rRNA gene sequences extracted with the PCR primer sequences from the QIIME-compatible, 99% identity-clustered SILVA v132 database (101). ASVs were classified by taxon using the fitted classifier (102). One hundred nine ASVs classified as chloroplasts or mitochondria were removed with on average 21% (0% to 95%) relative abundance per sample, and the remaining 3,388 ASVs with 6,107 to 139,201 (average 78,635) counts per sample had their abundances extracted by feature-table (103).

Statistical analysis. Statistical analyses were performed in R 4.1.0 using function p.adjust. Differences in the obtained results of DNA- and RNA-based relative abundances of planktonic (triplicate samples), particle-associated (triplicate samples), and benthic (duplicate samples) microbial taxa were evaluated using the Kruskal-Wallis test (52) with Benjamini-Hochberg correction (53).

Elemental analysis of liquid samples. The concentration of HMs in the river water (filtered with a 0.45-μm-pore-size syringe filter and stabilized with HNO_3) was analyzed with inductively coupled plasma-optical emission spectrometry (ICP-OES) (Spectroblue TI; Ametek). Dissolved Fe(II) and total Fe in river water were quantified by the ferrozine assay using a spectrophotometric plate reader (FlashScan 550; Analytic, Jena, Germany) (104). For calculation of Fe(III), the concentration of Fe(II) was subtracted from the total Fe concentration. Dissolved anions (NO_3^-, Cl^-, PO_4^{3-}, and SO_4^{2-}) in the water samples were quantified using a Dionex DX-120 ion chromatograph (Thermo, USA).

Geochemical modeling of the precipitation event occurring in the upper estuary. The saturation indices (SIs) were calculated using the modeling program PHREEQC and the WATEQ4F thermodynamic database. The hydrochemical characteristics of river water determined in the middle course and seawater characteristics determined in a previous study (105) were used as input parameters (Table S5). Based on this, seawater was calculated to account for 83% and 34% of estuarine water at high and low tide, respectively. The calculation of the mixing ratio of river and seawater was published earlier (21).

Elemental analysis of SPM. Closed microwave digestion was performed in a microwave system (Anton Paar Ltd. mod. multiwave GO Microwave digestion system). For analysis, each membrane filter was placed in a modified polytetrafluoroethylene (PTFE-TFM) digestion vessel. To each digestion vessel, 7.5 mL 37% HCl and 2.5 mL 65% HNO_3 were added. Two blank vessels without samples but with equal volumes of HCl and HNO_3 were also prepared for each digesting run. The following temperature gradient parameters were applied: step 1, ramping for 20 min to a maximum of 175°C (8.75°C/min); step 2, holding for 30 min at 175°C; and step 3, ventilation for 20 min to 50°C. After digestion, samples were adjusted to 50 mL with Milli-Q H_2O and stored in the dark prior to analysis. The content of HMs in the digests of SPM was analyzed with ICP-OES (Spectroblue TI; Ametek).

Mineralogical analysis of sediment samples. The red plaques (ES-RP) identified in the sediment ES4 at the upper estuary were retrieved, dried at room temperature, cleaned, and ground in a mortar. The resulting powder was analyzed on a 2D microdiffractometer (D8 Discover with GADDS [general area detector diffraction system], μ-XRD; Bruker AXS GmbH, Karlsruhe, Germany), using a cobalt anode tube as the X-ray source with a Co-Kα wavelength of 1.79030 Å and a 2D detector with a 40° angle cover (VÅNTEC-500; Bruker AXS GmbH, Karlsruhe, Germany). The sample was not rotated, and the reflection patterns were collected for 120 s per angle setting. Reflection pattern analysis and mineral identification were caried out using the Match! program for phase identification from powder diffraction (Match!; Crystal Impact, Bonn, Germany).

Data availability. Raw sequencing data have been deposited at the Sequencing Read Archive (SRA) under BioProject accession number PRJNA699454 (https://www.ncbi.nlm.nih.gov/bioproject/). Included were two previously published samples, SRR9028811 and SRR9028812 of PRJNA541861, used here for the calculation of the average value of relative abundance for DNA-based planktonic and particle-associated fractions (Fig. 3), which were filtered (0.22 μm and 8 μm, respectively) from the middle-course stream water of the Rio Tinto on 30 July 2017 (21).

SUPPLEMENTAL MATERIAL

Supplemental material is available online only.

SUPPLEMENTAL FILE 1, PDF file, 3.4 MB.

SUPPLEMENTAL FILE 2, XLSX file, 0.02 MB.

SUPPLEMENTAL FILE 3, XLSX file, 0.04 MB.

REFERENCES

1. Amils R. 2016. Lessons learned from thirty years of geomicrobiological studies of Rio Tinto. Res Microbiol 167:539–545. https://doi.org/10.1016/j.resmic.2016.06.001.
2. Amils R, Fernández-Remolar D, the IPBSL Team. 2014. Rio Tinto: aA geochemical and mineralogical terrestrial analogue of Mars. Life 4:511–534. https://doi.org/10.3390/life4030511.
3. Amils R, González-Toril E, Fernández-Remolar D, Gómez F, Aguilera Á, Rodríguez N, Malki M, García-Moyano A, Fairén AG, de la Fuente V, Luis Sanz J. 2007. Extreme environments as Mars terrestrial analogs: the Rio Tinto case. Planet Space Sci 55:370–381. https://doi.org/10.1016/j.pss.2006.02.006.
4. Fernández-Remolar DC, Prieto-Ballesteros O, Rodríguez N, Gómez F, Amils R, Gómez-Elvira J, Stoker CR. 2008. Underground habitats in the Río Tinto basin: a model for subsurface life habitats on Mars. Astrobiology 8:1023–1047. https://doi.org/10.1089/ast.2006.0104.
5. Amils R, Gonzalez-Toril E, Aguilera A, Rodriguez N, Fernandez-Remolar D, Gomez F, Garcia-Moyano A, Malki M, Oggerin M, Sanchez-Andrea I, Sanz JL. 2011. From Rio Tinto to Mars. The terrestrial and extraterrestrial ecology of acidophiles. Adv Appl Microbiol 77:41–70. https://doi.org/10.1016/B978-0-12-387044-5.00002-9.
6. Oggerin M, Tornos F, Rodriguez N, Pascual L, Amils R. 2016. Fungal iron biomineralization in Rio Tinto. Minerals 6:37. https://doi.org/10.3390/min6020037.
7. Duquesne K, Lebrun S, Casiot C, Bruneel O, Personné J-C, Leblanc M, Elbaz-Poulichet F, Morin G, Bonnefoy V. 2003. Immobilization of arsenite and ferric iron by *Acidithiobacillus ferrooxidans* and its relevance to acid mine drainage. Appl Environ Microbiol 69:6165–6173. https://doi.org/10.1128/AEM.69.10.6165-6173.2003.
8. Sánchez-España J, Yusta I, Burgos WD. 2016. Geochemistry of dissolved aluminum at low pH: hydrobasaluminite formation and interaction with trace metals, silica and microbial cells under anoxic conditions. Chem Geol 441:124–137. https://doi.org/10.1016/j.chemgeo.2016.08.004.
9. Sánchez-España J, Yusta I, Gray J, Burgos WD. 2016. Geochemistry of dissolved aluminum at low pH: extent and significance of Al–Fe(III) coprecipitation below pH 4.0. Geochim Cosmochim Acta 175:128–149. https://doi.org/10.1016/j.gca.2015.10.035.
10. Sánchez-Román M, Fernández-Remolar D, Amils R, Sánchez-Navas A, Schmid T, Martin-Uriz PS, Rodriguez N, McKenzie JA, Vasconcelos C. 2014. Microbial mediated formation of Fe-carbonate minerals under extreme acidic conditions. Sci Rep 4:4767. https://doi.org/10.1038/srep04767.
11. Bigham JM, Schwertmann U, Traina SJ, Winland RL, Wolf M. 1996. Schwertmannite and the chemical modeling of iron in acid sulfate waters. Geochim Cosmochim Acta 60:2111–2121. https://doi.org/10.1016/0016-7037(96)00091-9.
12. Dold B. 2014. Evolution of acid mine drainage formation in sulphidic mine tailings. Minerals 4:621–641. https://doi.org/10.3390/min4030621.
13. Cánovas CR, Olías M, Nieto JM, Sarmiento AM, Cerón JC. 2007. Hydrogeochemical characteristics of the Tinto and Odiel Rivers (SW Spain). Factors controlling metal contents. Sci Total Environ 373:363–382. https://doi.org/10.1016/j.scitotenv.2006.11.022.

14. Smith KS. 1997. Metal sorption on mineral surfaces: an overview with examples relating to mineral deposits, p 371. *In* Plumlee GS, Logsdon MJ, Filipek LF (ed), The environmental geochemistry of mineral deposits. Part A: processes, techniques, and health issues. Part B: case studies and research topics, vol 6. Society of Economic Geologists, Littleton, CO.
15. Duffus JH. 2002. "Heavy metals" a meaningless term? (IUPAC Technical Report). Pure Appl Chem 74:793–807. https://doi.org/10.1351/pac200274050793.
16. Tchounwou PB, Yedjou CG, Patlolla AK, Sutton DJ. 2012. Heavy metal toxicity and the environment. Exp Suppl 101:133–164. https://doi.org/10.1007/978-3-7643-8340-4_6.
17. van Geen A, Adkins JF, Boyle EA, Nelson CH, Palanques A. 1997. A 120-yr record of widespread contamination from mining of the Iberian pyrite belt. Geology 25:291–294. https://doi.org/10.1130/0091-7613(1997)025<0291:AYROWC>2.3.CO;2.
18. Baconnais I, Rouxel O, Dulaquais G, Boye M. 2019. Determination of the copper isotope composition of seawater revisited: a case study from the Mediterranean Sea. Chem Geol 511:465–480. https://doi.org/10.1016/j.chemgeo.2018.09.009.
19. Koski RA. 2012. Metal dispersion resulting from mining activities in coastal environments: a pathways approach. Oceanograpgy 25:170–183. https://doi.org/10.5670/oceanog.2012.53.
20. Olías M, Cánovas CR, Macías F, Basallote MD, Nieto JM. 2020. The evolution of pollutant concentrations in a river severely affected by acid mine drainage: Rio Tinto (SW Spain). Minerals 10:598. https://doi.org/10.3390/min10070598.
21. Abramov SM, Tejada J, Grimm L, Schädler F, Bulaev A, Tomaszewski EJ, Byrne JM, Straub D, Thorwarth H, Amils R, Kleindienst S, Kappler A. 2020. Role of biogenic Fe(III) minerals as a sink and carrier of heavy metals in the Rio Tinto, Spain. Sci Total Environ 718:137294. https://doi.org/10.1016/j.scitotenv.2020.137294.
22. Neff JM. 2002. Chromium in the ocean, p 131–143. *In* Neff JM (ed), Bioaccumulation in marine organisms. Elsevier, Oxford, United Kingdom.
23. Yilmaz A, Yanar A, Alkan E. 2018. Review of heavy metal accumulation in aquatic environment of Northern East Mediterrenean Sea part II: some non-essential metals. Pollution 4:143–181.
24. Cánovas CR, Olias M, Vazquez-Suñé E, Ayora C, Nieto JM. 2012. Influence of releases from a fresh water reservoir on the hydrochemistry of the Tinto River (SW Spain). Sci Total Environ 416:418–428. https://doi.org/10.1016/j.scitotenv.2011.11.079.
25. Usero J, Izquierdo C, Morillo J, Gracia I. 2004. Heavy metals in fish (*Solea vulgaris*, *Anguilla anguilla* and *Liza aurata*) from salt marshes on the southern Atlantic coast of Spain. Environ Int 29:949–956. https://doi.org/10.1016/S0160-4120(03)00061-8.
26. Vicente-Martorell JJ, Galindo-Riaño MD, García-Vargas M, Granado-Castro MD. 2009. Bioavailability of heavy metals monitoring water, sediments and fish species from a polluted estuary. J Hazard Mater 162:823–836. https://doi.org/10.1016/j.jhazmat.2008.05.106.

27. Elbaz-Poulichet F, Leblanc M, Borrego J, Morales JA. 2000. 4,500-year-old mining pollution in Southwestern Spain: long-term implications for modern mining pollution. Econ Geol 95:655–662.

28. Braungardt CB, Achterberg EP, Elbaz-Poulichet F, Morley NH. 2003. Metal geochemistry in a mine-polluted estuarine system in Spain. Appl Geochem 18:1757–1771. https://doi.org/10.1016/S0883-2927(03)00079-9.

29. Cánovas CR, Olías M, Sarmiento AM, Nieto JM, Galván L. 2012. Pollutant transport processes in the Odiel River (SW Spain) during rain events. Water Resour Res 48:W06508. https://doi.org/10.1029/2011WR011041.

30. Achterberg EP, Herzl VMC, Braungardt CB, Millward GE. 2003. Metal behaviour in an estuary polluted by acid mine drainage: the role of particulate matter. Environ Pollut 121:283–292. https://doi.org/10.1016/S0269-7491(02)00216-6.

31. Elbaz-Poulichet F, Braungardt C, Achterberg E, Morley N, Cossa D, Beckers J-M, Nomérange P, Cruzado A, Leblanc M. 2001. Metal biogeochemistry in the Tinto–Odiel rivers (southern Spain) and in the Gulf of Cadiz: a synthesis of the results of TOROS project. Continent Shelf Res 21:1961–1973. https://doi.org/10.1016/S0278-4343(01)00037-1.

32. García-Moyano A, Gonzalez-Toril E, Moreno-Paz M, Parro Garcia V, Amils R. 2007. Microbial ecology of *Leptospirillum* spp. in Río Tinto, a model of interest to biohydrometallurgy. Adv Mater Res 20-21:409–412. https://doi.org/10.4028/www.scientific.net/AMR.20-21.409.

33. González-Toril E, Aguilera A. 2019. Microbial ecology in extreme acidic environments: use of molecular tools, p 227–238. *In* Das S, Dash HR (ed), Microbial diversity in the genomic era. Academic Press, New York, NY.

34. Fernández-Remolar DC, Morris RV, Gruener JE, Amils R, Knoll AH. 2005. The Río Tinto basin, Spain: mineralogy, sedimentary geobiology, and implications for interpretation of outcrop rocks at Meridiani Planum, Mars. Earth Planet Sci Lett 240:149–167. https://doi.org/10.1016/j.epsl.2005.09.043.

35. Liu H, Yin H, Dai Y, Dai Z, Liu Y, Li Q, Jiang H, Liu X. 2011. The co-culture of *Acidithiobacillus ferrooxidans* and *Acidiphilium acidophilum* enhances the growth, iron oxidation, and CO_2 fixation. Arch Microbiol 193:857–866. https://doi.org/10.1007/s00203-011-0723-8.

36. Falagan C, Johnson DB. 2014. *Acidibacter ferrireducens* gen. nov., sp. nov.: an acidophilic ferric iron-reducing gammaproteobacterium. Extremophiles 18:1067–1073. https://doi.org/10.1007/s00792-014-0684-3.

37. Johnson DB, Kanao T, Hedrich S. 2012. Redox transformations of iron at extremely low pH: fundamental and applied aspects. Front Microbiol 3:96. https://doi.org/10.3389/fmicb.2012.00096.

38. Luef B, Aspetsberger F, Hein T, Huber F, Peduzzi P. 2007. Impact of hydrology on free-living and particle-associated microorganisms in a river floodplain system (Danube, Austria). Freshwater Biol 52:1043–1057. https://doi.org/10.1111/j.1365-2427.2007.01752.x.

39. Schweitzer-Natan O, Ofek-Lalzar M, Sher D, Sukenik A. 2019. Particle-associated microbial community in a subtropical lake during thermal mixing and phytoplankton succession. Front Microbiol 10:2142. https://doi.org/10.3389/fmicb.2019.02142.

40. Davis RA, Jr, Welty AT, Borrego J, Morales JA, Pendon JG, Ryan JG. 2000. Rio Tinto estuary (Spain): 5000 years of pollution. Environ Geol 39:1107–1116. https://doi.org/10.1007/s002549900096.

41. Borrego J, Morales J, de la Torre M, Grande J. 2002. Geochemical characteristics of heavy metal pollution in surface sediments of the Tinto and Odiel river estuary (southwestern Spain). Environ Geol 41:785–796. https://doi.org/10.1007/s00254-001-0445-3.

42. de la Torre ML, Sánchez-Rodas D, Grande JA, Gomez T. 2010. Relationships between pH, colour and heavy metal concentrations in the Tinto and Odiel rivers (southwest Spain). Hydrol Res 41:406–413. https://doi.org/10.2166/nh.2010.082.

43. Hierro A, Olías M, Cánovas CR, Martín JE, Bolivar JP. 2014. Trace metal partitioning over a tidal cycle in an estuary affected by acid mine drainage (Tinto estuary, SW Spain). Sci Total Environ 497-498:18–28. https://doi.org/10.1016/j.scitotenv.2014.07.070.

44. Carro B, Borrego J, Morales JA. 2019. Estuaries of the Huelva coast: Odiel and Tinto estuaries (SW Spain), p 543–564. *In* Morales JA (ed), The spanish coastal systems. Springer International Publishing, Cham, Switzerland.

45. Lu S, Peiffer S, Lazar CS, Oldham C, Neu TR, Ciobota V, Nab O, Lillicrap A, Rösch P, Popp J, Küsel K. 2016. Extremophile microbiomes in acidic and hypersaline river sediments of Western Australia. Environ Microbiol Rep 8:58–67. https://doi.org/10.1111/1758-2229.12351.

46. Eduardo-Correia B, Morales-Filloy H, Abad JP. 2019. Bacteria from the multi-contaminated Tinto River estuary (SW, Spain) show high multi-resistance to antibiotics and point to *Paenibacillus* spp. as antibiotic-resistance-dissemination players. Front Microbiol 10:3071. https://doi.org/10.3389/fmicb.2019.03071.

47. Li R, Tun HM, Jahan M, Zhang Z, Kumar A, Dilantha Fernando WG, Farenhorst A, Khafipour E. 2017. Comparison of DNA-, PMA-, and RNA-based 16S rRNA Illumina sequencing for detection of live bacteria in water. Sci Rep 7:5752. https://doi.org/10.1038/s41598-017-02516-3.

48. Salgar-Chaparro SJ, Machuca LL. 2019. Complementary DNA/RNA-based profiling: characterization of corrosive microbial communities and their functional profiles in an oil production facility. Front Microbiol 10:2587. https://doi.org/10.3389/fmicb.2019.02587.

49. Moeseneder MM, Arrieta JM, Herndl GJ. 2005. A comparison of DNA- and RNA-based clone libraries from the same marine bacterioplankton community. FEMS Microbiol Ecol 51:341–352. https://doi.org/10.1016/j.femsec.2004.09.012.

50. Lillis L, Doyle E, Clipson N. 2009. Comparison of DNA- and RNA-based bacterial community structures in soil exposed to 2,4-dichlorophenol. J Appl Microbiol 107:1883–1893. https://doi.org/10.1111/j.1365-2672.2009.04369.x.

51. Kim TG, Moon K-E, Yun J, Cho K-S. 2013. Comparison of RNA- and DNA-based bacterial communities in a lab-scale methane-degrading biocover. Appl Microbiol Biotechnol 97:3171–3181. https://doi.org/10.1007/s00253-012-4123-z.

52. Kruskal WH, Wallis WA. 1952. Use of ranks in one-criterion variance analysis. J Am Stat Assoc 47:583–621. https://doi.org/10.1080/01621459.1952.10483441.

53. Benjamini Y, Hochberg Y. 1995. Controlling the false discovery rate: a practical and powerful approach to multiple testing. J R Stat Soc Ser B 57:289–300. https://doi.org/10.1111/j.2517-6161.1995.tb02031.x.

54. Das GK, Acharya S, Anand S, Das RP. 1996. Jarosites: a review. Miner Process Extract Metal Rev 16:185–210. https://doi.org/10.1080/08827509708914135.

55. Morgan B, Lahav O. 2007. The effect of pH on the kinetics of spontaneous Fe(II) oxidation by O_2 in aqueous solution—basic principles and a simple heuristic description. Chemosphere 68:2080–2084. https://doi.org/10.1016/j.chemosphere.2007.02.015.

56. Falagán C, Johnson DB. 2018. The significance of pH in dictating the relative toxicities of chloride and copper to acidophilic bacteria. Res Microbiol 169:552–557. https://doi.org/10.1016/j.resmic.2018.07.004.

57. Casiot C, Morin G, Juillot F, Bruneel O, Personné J-C, Leblanc M, Duquesne K, Bonnefoy V, Elbaz-Poulichet F. 2003. Bacterial immobilization and oxidation of arsenic in acid mine drainage (Carnoulès Creek, France). Water Res 37:2929–2936. https://doi.org/10.1016/S0043-1354(03)00080-0.

58. Sholkovitz ER. 1976. Flocculation of dissolved organic and inorganic matter during the mixing of river water and seawater. Geochim Cosmochim Acta 40:831–845. https://doi.org/10.1016/0016-7037(76)90035-1.

59. Mosley LM, Liss PS. 2020. Particle aggregation, pH changes and metal behaviour during estuarine mixing: review and integration. Mar Freshw Res 71:300–310. https://doi.org/10.1071/MF19195.

60. Carro B, Borrego J, Lopez-Gonzalez N, Gomez T, Torre ML, Valente T. 2011. Impact of acid mine drainage on the hydrogeochemical characteristics of the Tinto-Odiel estuary (SW Spain). J Iberian Geology 37:87–96.

61. Rumin AI, Mironkina NV. 2013. Study of dissolution kinetics of lead sulfate in solutions of sodium chloride and sodium hydrate. J Siber Fed Univ Eng Technol 6:450–454.

62. Byrne RH, Yao W, Luo Y, Millero FJ. 2010. Complexation of Pb(II) by chloride ions in aqueous solutions. Aquat Geochem 16:325–335. https://doi.org/10.1007/s10498-010-9101-4.

63. Fernández-Remolar DC, Rodriguez N, Gómez F, Amils R. 2003. Geological record of an acidic environment driven by iron hydrochemistry: the Tinto River system. J Geophys Res 108. https://doi.org/10.1029/2002JE001918.

64. Torti A, Jørgensen BB, Lever MA. 2018. Preservation of microbial DNA in marine sediments: insights from extracellular DNA pools. Environ Microbiol 20:4526–4542. https://doi.org/10.1111/1462-2920.14401.

65. Torres-Beltrán M, Mueller A, Scofield M, Pachiadaki MG, Taylor C, Tyshchenko K, Michiels C, Lam P, Ulloa O, Jürgens K, Hyun J-H, Edgcomb VP, Crowe SA, Hallam SJ. 2019. Sampling and processing methods impact microbial community structure and potential activity in a seasonally anoxic fjord: Saanich Inlet, British Columbia. Front Mar Sci 6:132. https://doi.org/10.3389/fmars.2019.00132.

66. Cárdenas JP, Moya F, Covarrubias P, Shmaryahu A, Levicán G, Holmes DS, Quatrini R. 2012. Comparative genomics of the oxidative stress response in bioleaching microorganisms. Hydrometallurgy 127-128:162–167. https://doi.org/10.1016/j.hydromet.2012.07.014.

67. Cortés A, Flores R, Norambuena J, Cárdenas J, Quatrini R, Chavez R, Orellana O, Levican G. 2011. Comparative study of redox stress response in the acidophilic bacteria *Leptospirillum ferriphilum* and *Acidithiobacillus ferrooxidans*, p 354–357. 19th International Biohydrometallurgy Symposium.

68. Rawlings DE, Tributsch H, Hansford GS. 1999. Reasons why '*Leptospirillum*'-like species rather than *Thiobacillus ferrooxidans* are the dominant

iron-oxidizing bacteria in many commercial processes for the biooxidation of pyrite and related ores. Microbiology 145:5–13. https://doi.org/10.1099/13500872-145-1-5.

69. Ebrahimi S, Faraghi N, Hosseini M. 2015. Model-based evaluation of ferrous iron oxidation by acidophilic bacteria in chemostat and biofilm airlift reactors. J Ind Microbiol Biotechnol 42:1363–1368. https://doi.org/10.1007/s10295-015-1667-9.

70. van Scherpenzeel DA, Boon M, Ras C, Hansford GS, Heijnen JJ. 1998. Kinetics of ferrous iron oxidation by *Leptospirillum* bacteria in continuous cultures. Biotechnol Prog 14:425–433. https://doi.org/10.1021/bp980016h.

71. Issotta F, Moya-Beltrán A, Mena C, Covarrubias PC, Thyssen C, Bellenberg S, Sand W, Quatrini R, Vera M. 2018. Insights into the biology of acidophilic members of the *Acidiferrobacteraceae* family derived from comparative genomic analyses. Res Microbiol 169:608–617. https://doi.org/10.1016/j.resmic.2018.08.001.

72. Johnson DB. 2012. Geomicrobiology of extremely acidic subsurface environments. FEMS Microbiol Ecol 81:2–12. https://doi.org/10.1111/j.1574-6941.2011.01293.x.

73. Coupland K, Johnson DB. 2008. Evidence that the potential for dissimilatory ferric iron reduction is widespread among acidophilic heterotrophic bacteria. FEMS Microbiol Lett 279:30–35. https://doi.org/10.1111/j.1574-6968.2007.00998.x.

74. Heinhorst S, Baker SH, Johnson DR, Davies PS, Cannon GC, Shively JM. 2002. Two copies of form I RuBisCO genes in *Acidithiobacillus ferrooxidans* ATCC 23270. Curr Microbiol 45:115–117. https://doi.org/10.1007/s00284-001-0094-5.

75. Küsel K, Roth U, Drake HL. 2002. Microbial reduction of Fe(III) in the presence of oxygen under low pH conditions. Environ Microbiol 4:414–421. https://doi.org/10.1046/j.1462-2920.2002.00314.x.

76. Johnson DB, McGinness S. 1991. Ferric iron reduction by acidophilic heterotrophic bacteria. Appl Environ Microbiol 57:207–211. https://doi.org/10.1128/aem.57.1.207-211.1991.

77. Küsel K, Dorsch T, Acker G, Stackebrandt E. 1999. Microbial reduction of Fe(III) in acidic sediments: isolation of Acidiphilium cryptum JF-5 capable of coupling the reduction of Fe(III) to the oxidation of glucose. Appl Environ Microbiol 65:3633–3640. https://doi.org/10.1128/AEM.65.8.3633-3640.1999.

78. Peiffer S, Oldham C, Salmon U, Lillicrap A, Küsel K. 2009. Does iron cycling trigger generation of acidity in groundwaters of Western Australia? Environ Sci Technol 43:6548–6552. https://doi.org/10.1021/es9001086.

79. Zammit CM, Mangold S, Rao Jonna V, Mutch LA, Watling HR, Dopson M, Watkin ELJ. 2012. Bioleaching in brackish waters—effect of chloride ions on the acidophile population and proteomes of model species. Appl Microbiol Biotechnol 93:319–329. https://doi.org/10.1007/s00253-011-3731-3.

80. López-González N, Borrego J, Morales JA, Carro B, Lozano-Soria O. 2006. Metal fractionation in oxic sediments of an estuary affected by acid mine drainage (south-western Spain). Estuar Coast Shelf Sci 68:297–304. https://doi.org/10.1016/j.ecss.2006.01.020.

81. Bertel D, Peck J, Quick TJ, Senko JM. 2012. Iron transformations induced by an acid-tolerant *Desulfosporosinus* species. Appl Environ Microbiol 78:81–88. https://doi.org/10.1128/AEM.06337-11.

82. Gao K, Jiang M, Guo C, Zeng Y, Fan C, Zhang J, Reinfelder JR, Huang W, Lu G, Dang Z. 2019. Reductive dissolution of jarosite by a sulfate reducing bacterial community: secondary mineralization and microflora development. Sci Total Environ 690:1100–1109. https://doi.org/10.1016/j.scitotenv.2019.06.483.

83. Gramp JP, Wang H, Bigham JM, Jones FS, Tuovinen OH. 2009. Biogenic synthesis and reduction of Fe(III)-hydroxysulfates. Geomicrobiol J 26:275–280. https://doi.org/10.1080/01490450902892597.

84. Sánchez-Andrea I, Rodríguez N, Amils R, Sanz JL. 2011. Microbial diversity in anaerobic sediments at Río Tinto, a naturally acidic environment with a high heavy metal content. Appl Environ Microbiol 77:6085–6093. https://doi.org/10.1128/AEM.00654-11.

85. Fukushi K, Sasaki M, Sato T, Yanase N, Amano H, Ikeda H. 2003. A natural attenuation of arsenic in drainage from an abandoned arsenic mine dump. Appl Geochem 18:1267–1278. https://doi.org/10.1016/S0883-2927(03)00011-8.

86. García-Moyano A, González-Toril E, Aguilera Á, Amils R. 2012. Comparative microbial ecology study of the sediments and the water column of the Río Tinto, an extreme acidic environment. FEMS Microbiol Ecol 81:303–314. https://doi.org/10.1111/j.1574-6941.2012.01346.x.

87. Osorio H, Mettert E, Kiley P, Dopson M, Jedlicki E, Holmes DS. 2019. Identification and unusual properties of the master regulator FNR in the extreme acidophile *Acidithiobacillus ferrooxidans*. Front Microbiol 10:1642. https://doi.org/10.3389/fmicb.2019.01642.

88. Nelson CH, Lamothe PJ. 1993. Heavy metal anomalies in the Tinto and Odiel River and estuary system, Spain. Estuaries 16:496–511. https://doi.org/10.2307/1352597.

89. Illuminati S, Annibaldi A, Truzzi C, Tercier-Waeber M-L, Nöel S, Braungardt CB, Achterberg EP, Howell KA, Turner D, Marini M, Romagnoli T, Totti C, Confalonieri F, Graziottin F, Buffle J, Scarponi G. 2019. In-situ trace metal (Cd, Pb, Cu) speciation along the Po River plume (Northern Adriatic Sea) using submersible systems. Mar Chem 212:47–63. https://doi.org/10.1016/j.marchem.2019.04.001.

90. Castro L, Blázquez ML, González F, Muñoz JA, Ballester A. 2019. Anaerobic bioreduction of jarosites and biofilm formation by a natural microbial consortium. Minerals 9:81. https://doi.org/10.3390/min9020081.

91. R Core Team. 2018. R: a language and environment for statistical computing. R Foundation for Statistical Computing, Vienna, Austria. https://www.R-project.org/.

92. Lueders T, Manefield M, Friedrich MW. 2004. Enhanced sensitivity of DNA- and rRNA-based stable isotope probing by fractionation and quantitative analysis of isopycnic centrifugation gradients. Environ Microbiol 6:73–78. https://doi.org/10.1046/j.1462-2920.2003.00536.x.

93. Caporaso JG, Kuczynski J, Stombaugh J, Bittinger K, Bushman FD, Costello EK, Fierer N, Peña AG, Goodrich JK, Gordon JI, Huttley GA, Kelley ST, Knights D, Koenig JE, Ley RE, Lozupone CA, McDonald D, Muegge BD, Pirrung M, Reeder J, Sevinsky JR, Turnbaugh PJ, Walters WA, Widmann J, Yatsunenko T, Zaneveld J, Knight R. 2010. QIIME allows analysis of high-throughput community sequencing data. Nat Methods 7:335–336. https://doi.org/10.1038/nmeth.f.303.

94. Straub D, Blackwell N, Langarica-Fuentes A, Peltzer A, Nahnsen S, Kleindienst S. 2020. Interpretations of environmental microbial community studies are biased by the selected 16S rRNA (gene) amplicon sequencing pipeline. Front Microbiol 11:2652. https://doi.org/10.3389/fmicb.2020.550420.

95. Ewels PA, Peltzer A, Fillinger S, Patel H, Alneberg J, Wilm A, Garcia MU, Di Tommaso P, Nahnsen S. 2020. The nf-core framework for community-curated bioinformatics pipelines. Nat Biotechnol 38:276–278. https://doi.org/10.1038/s41587-020-0439-x.

96. Di Tommaso P, Chatzou M, Floden EW, Barja PP, Palumbo E, Notredame C. 2017. Nextflow enables reproducible computational workflows. Nat Biotechnol 35:316–319. https://doi.org/10.1038/nbt.3820.

97. Kurtzer GM, Sochat V, Bauer MW. 2017. Singularity: scientific containers for mobility of compute. PLoS One 12:e0177459. https://doi.org/10.1371/journal.pone.0177459.

98. Martin M. 2011. Cutadapt removes adapter sequences from high-throughput sequencing reads. EMBnet J 17:10–12. https://doi.org/10.14806/ej.17.1.200.

99. Bolyen E, Rideout JR, Dillon MR, Bokulich NA, Abnet CC, Al-Ghalith GA, Alexander H, Alm EJ, Arumugam M, Asnicar F, Bai Y, Bisanz JE, Bittinger K, Brejnrod A, Brislawn CJ, Brown CT, Callahan BJ, Caraballo-Rodríguez A, Mauricio Chase J, Cope EK, Da Silva R, Diener C, Dorrestein PC, Douglas GM, Durall DM, Duvallet C, Edwardson CF, Ernst M, Estaki M, Fouquier J, Gauglitz JM, Gibbons SM, Gibson DL, Gonzalez A, Gorlick K, Guo J, Hillmann B, Holmes S, Holste H, Huttenhower C, Huttley GA, Janssen S, Jarmusch AK, Jiang L, Kaehler BD, Kang KB, Keefe CR, Keim P, Kelley ST, Knights D, et al. 2019. Reproducible, interactive, scalable and extensible microbiome data science using QIIME 2. Nat Biotechnol 37:852–857. https://doi.org/10.1038/s41587-019-0209-9.

100. Callahan BJ, McMurdie PJ, Rosen MJ, Han AW, Johnson AJ, Holmes SP. 2016. DADA2: high-resolution sample inference from Illumina amplicon data. Nat Methods 13:581–583. https://doi.org/10.1038/nmeth.3869.

101. Pruesse E, Quast C, Knittel K, Fuchs BM, Ludwig W, Peplies J, Glöckner FO. 2007. SILVA: a comprehensive online resource for quality checked and aligned ribosomal RNA sequence data compatible with ARB. Nucleic Acids Res 35:7188–7196. https://doi.org/10.1093/nar/gkm864.

102. Bokulich NA, Kaehler BD, Rideout JR, Dillon M, Bolyen E, Knight R, Huttley GA, Gregory Caporaso J. 2018. Optimizing taxonomic classification of marker-gene amplicon sequences with QIIME 2's q2-feature-classifier plugin. Microbiome 6:90. https://doi.org/10.1186/s40168-018-0470-z.

103. McDonald D, Clemente JC, Kuczynski J, Rideout JR, Stombaugh J, Wendel D, Wilke A, Huse S, Hufnagle J, Meyer F, Knight R, Caporaso JG. 2012. The Biological Observation Matrix (BIOM) format or: how I learned to stop worrying and love the ome-ome. Gigascience 1:7. https://doi.org/10.1186/2047-217X-1-7.

104. Stookey LL. 1970. Ferrozine—a new spectrophotometric reagent for iron. Anal Chem 42:779–781. https://doi.org/10.1021/ac60289a016.

105. Millero FJ. 1974. The physical chemistry of seawater. Annu Rev Earth Planet Sci 2:101–150. https://doi.org/10.1146/annurev.ea.02.050174.000533.